Diet and temperature interactively impact brown adipose tissue gene regulation controlled by DNA methylation

Tobias Hagemann[1,*], Anne Hoffmann[1,*], Kerstin Rohde-Zimmermann[1,*], Helen Broghammer[1], Lucas Massier[1,2], Peter Kovacs[3], Michael Stumvoll[1,3], Matthias Blüher[1,3], John T. Heiker[1,3,*, §] & Juliane Weiner[1,3,*, §]

[1]Helmholtz Institute for Metabolic, Obesity and Vascular Research (HI-MAG) of the Helmholtz Zentrum München at the University of Leipzig and University Hospital Leipzig, Leipzig, Germany
[2]Department of Medicine H7, Karolinska Institutet, Stockholm, Sweden
[3]Leipzig University Medical Center, Divisions of Endocrinology and Nephrology, University of Leipzig, Leipzig, Germany

*These authors contribute equally

[§]**Corresponding authors:**
Juliane Weiner
[2]Leipzig University Medical Center, Divisions of Endocrinology and Nephrology, University of Leipzig, Leipzig, Germany,
Liebigstr. 21, D-04103 Leipzig, Germany
Email: Juliane.Weiner@medizin.uni-leipzig.de
Phone: +49-341-97 20919

John T. Heiker
Helmholtz Institute for Metabolic, Obesity and Vascular Research (HI-MAG)
Helmholtz Zentrum München at the University of Leipzig and University Hospital Leipzig
Philipp-Rosenthal-Straße 27, D-04103 Leipzig, Germany
Email: John.Heiker@helmholtz-munich.de
Phone: +49-341-97 22909

Keywords: brown adipose tissue, DNA methylation, high fat diet, cold exposure, epigenetics

Abbreviations: Aza: 5'aza-2'-deoxycytidine (Aza), BAT: Brown adipose tissue, BH: Bonferroni-Holm, DEG: differentially expressed gene, DGE: differential gene expression, DMEG: Differentially methylated and expressed gene, DMP: differentially methylated positions, DMR: differentially methylated regions, eWAT: epididymal white adipose tissue, FC: fold change, FDR: false discovery rate, HFD: high-fat diet, imBA: immortalized brown adipocytes, iWAT: white adipose tissue, PCA: principal component analysis, qPCR: quantitative real-time-PCR, RNAseq: RNA sequencing, RRBS: reduced representation bisulfite sequencing, SAM: S-adenosylmethionine, SVF: stromal vascular fraction, VST: variance stabilization transformation

Abstract

Controlling brown adipose tissue (BAT) plasticity in adulthood holds promising potential for effective new obesity therapies by targeting the mechanisms of adaptive thermogenesis. Recent studies have shown that BAT development and function are under epigenetic control, with DNA methylation linked to the regulation of key thermogenic and metabolic genes. Here we sought to understand how diet and cold exposure interactively shape BAT gene regulation controlled by DNA methylation. Mice (N = 8 per group) were housed under cold exposure (8°C) or thermoneutrality (30°C) and fed either chow or high-fat diet (HFD). BAT was isolated for transcriptome (RNAseq) and methylome (RRBS) analyses. We identified differentially methylated and expressed genes (DMEGs) by comparing the effects of cold exposure under chow and high-fat diet, as well as by analyzing the interaction between temperature and diet. Functional pathway enrichment and EpiFactors Database screening were used to assess epigenetic regulators, and candidate gene expression was validated by modulating DNA-methylation in vitro. We identified ~1,360 differentially expressed genes (DEGs) uniquely affected by the diet-temperature interaction with most downregulated in HFD-fed mice, indicating that obesity limits the transcriptional response of BAT to cold. 65 DMEGs (4% of DEGs) were largely diet-specific in response to cold exposure, suggesting that DNA methylation contributes to a selective layer of gene regulation during BAT adaptation to distinct metabolic states. In HFD-fed mice, DMEGs were enriched in pathways related to mitochondrial dysfunction, altered lipid metabolism, neuroendocrine signaling, and compensatory stress responses, contrasting the adaptive thermogenic profile observed in chow-fed controls. Differentially expressed genes of epigenetic regulators such as *Tet2*, *Dnmt3a* and *Apobec1* showed diet- and cold-dependent regulation, indicating impaired methylation flexibility under obesogenic conditions. Using cell culture experiments, we confirmed the regulation of gene expression of candidate genes, validating the functional link between DNA methylation and thermogenic gene regulation. This is the first study to demonstrate an epigenetic response to cold exposure that differs by dietary condition, particularly in obesity. Our findings highlight a coordinated transcriptional and epigenetic remodeling of BAT, shaped by both environmental and metabolic signals. These insights may inform targeted epigenetic or nutritional strategies to restore BAT function and would further strengthen our understanding of how these might be used as therapeutic basis to improve metabolic health in obesity.

Graphical abstract

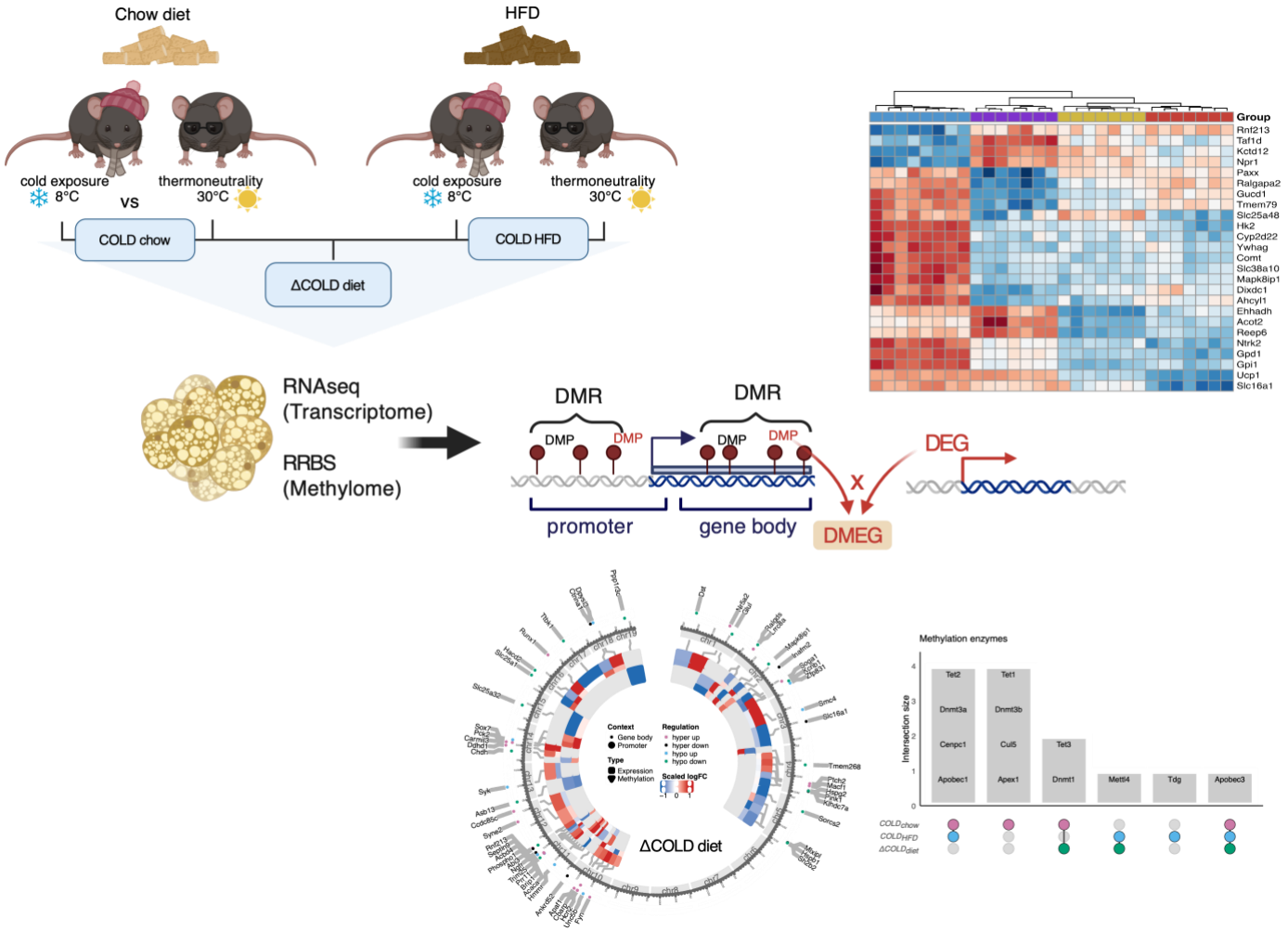

Mice were housed under cold exposure or thermoneutrality and fed either chow or high-fat diet (HFD). RNA sequencing (RNAseq) and reduced representation bisulfite sequencing (RRBS) was performed on brown adipose tissue (BAT) which provide the fundament for the identification of differentially methylated positions (DMP) and regions (DMR) as well as differentially expressed genes (DEG) in three models: $COLD_{chow}$, comparing 8° vs 30°C mice on chow diet; $COLD_{HFD}$, comparing 8° vs 30°C mice on HFD diet and $\Delta COLD_{diet}$, comparing $COLD_{chow}$ vs $COLD_{HFD}$. Differentially methylated and expressed genes (DMEGs; circos plot shows a representative example) were identified for all comparisons based on those DMPs which correlated significantly with differentially expressed genes (DEGs; the heatmap shows a representative example). DMEGs were taken forward for pathways enrichment analyses and to identify differentially regulated epigenetic regulators using the EpiFactors Database. The figure was created with BioRender.

1. Introduction

Brown adipose tissue (BAT) is a specialized fat tissue that is rich in mitochondria and promotes non-shivering thermogenesis by expressing the *uncoupling protein 1 (UCP1).* Unlike white adipose tissue, it burns calories to produce heat and therefore plays a key role in energy regulation and controlling metabolic health. Increasing energy expenditure by BAT activation is an intriguing therapeutic approach to combat the overwhelming obesity pandemic, either alone or to complement the current pharmacotherapy that mainly addresses energy intake based on the incretin-mimetic poly-agonist class of drugs [1]. With this in mind it is not surprising that a lot of research was conducted to understand the molecular underpinnings of BAT regulation specifically addressing environmental cues. Cold exposure is the most powerful inducer of BAT activation leading to the upregulation of thermogenic gene program and adrenergic receptor-mediated activation of lipolysis and metabolism. BAT activation also occurs post-prandially, especially after acute overfeeding, to trigger diet-induced thermogenesis [2,3]. However, this compensatory component of energy-expenditure is impaired during chronic overfeeding, a phenomenon that was termed adaptive thermogenesis, and is believed to further drive weight gain and obesity [2,4,5].

In any case the mechanistical switch enabling the high plasticity of BAT changing from passive thermoneutral to active thermogenic states may be regulated by epigenetic mechanisms that are affected by, e.g. temperature and diet [6]. Indeed, studies have shown changes in DNA methylation for key BAT regulatory genes such as *Ucp1, PR domain containing 16* (*Prdm16*) or *PPARG coactivator 1 alpha* (*Ppargc1a*) , altering their expression level and impacting BAT function [7,8]. Moreover, during the development of precursor cells into major brown adipocytes, DNA methylation patterns change and lineage commitment towards a thermogenic adipocyte is epigenetically controlled [8]. The major relevance of the ambient temperature in this context has just recently been implied, as cold exposure of parents at conception is related to increased brown adipogenesis and thermogenesis along with reduced obesity risk in the offspring [9]. Mechanistically, sperm DNA methylation is altered in response to cold exposure which leads to adaptations in BAT activity of the offspring [10,11]. In addition, DNA methylation in key genes of thermogenesis and fatty acid oxidation, such as *acetyl-CoA acyltransferase 2* (*Acaa2*) and *acyl-CoA synthetase long chain family member 1* (*Acsl1*), is increased in BAT of offsprings from mice fed a high fat diet [12]. These studies strongly imply the relevance of cold, diet and obesity on the transgenerational modulation of BAT function. However, these environmental cues, either alone or in combination, also trigger and control BAT plasticity during adulthood. Rats with a blockade in afferent vagal nerve signaling that triggered by high-fat diet showed a reduced BAT activation after cold exposure [13]. The relevance of diet for regulating DNA methylation in later life comes with nutritional compounds such as folate or methionine as critical components of the one-carbon metabolism, which are classically enriched in vegetable-rich diets but diminished in high fat diets.

However, the interaction of especially cold exposure and high fat diet on BAT's epigenetic machinery is less understood. In this study, we aimed to address DNA methylation alterations in response to temperature and diet, and link this to changes in gene expression of BAT in mice on a

genome-wide level. We explored the interactive impact of diet and cold exposure on the epigenetic regulation of BAT gene expression. Using a stringent bioinformatic workflow we focused on differentially methylated and expressed genes (DMEGs) by taking forward only candidates whose differential methylation signal correlates to the gene expression level in order to provide only top functional relevant candidates. Providing a profound overview over the impact of DNA methylation on genes expression affected by cold and diet is of strong relevance to understand adult BAT plasticity and adaptive thermogenesis and provides the fundament for new obesity treatment strategies.

2. Material and methods

2.1. Animal studies

Male C57BL/6NTac mice (Taconic Bioscience, Lille Skensved, Denmark) were housed in pathogen-free facilities at 23°C on a 12h light/dark cycle at the Sächsische Inkubator für Klinische Translation (SIKT), Leipzig. Starting from five weeks of age, mice were either fed a standard chow diet (EV153, 3.3% from fat, Ssniff, Soest, Germany) or a high fat diet (HFD, E15742, 60 kJ% from fat, Ssniff) with ad libitum access to food and water. At 11 (chow) or 22 (HFD) weeks of age, mice were adapted to single housing in rodent climate chambers (MKKL1200, Flohr Instruments, Netherlands) for 5 days, before randomization into four groups (each N = 8 mice) and housed either at thermoneutrality (30°C) or in the cold (8°C) for 7 days. After a 4-hour fasting period, body weight and rectal temperature were measured. BAT and tail surface temperatures were measured by thermal imaging (VarioCAM®, InfraTec, Dresden, Germany). Mice were sacrificed and tissue samples of intrascapular brown adipose tissue (BAT) were collected, snap frozen in liquid nitrogen and stored at -80°C before further analyses. All animal experiments were approved by the local authorities of the Free State of Saxony, Germany (Landesdirektion Leipzig: TVV51/20), as recommended by the responsible local animal ethics review board.

2.2. RNA sequencing of brown adipose tissue

RNA from BAT was isolated using RNeasy Lipid Tissue Mini kit (Qiagen, Hilden, Germany) as specified by the manufacturer. RNA sequencing (RNAseq) was performed by the core unit DNA-Technologien, Medical Faculty Leipzig. 50ng of total RNA were depleted of ribosomal RNA using the NEBNext rRNA Depletion Kit v2 (NEB, USA) according to the manufacturer's instructions. Depleted RNA was transcribed using SuperScript IV reverse transcriptase (ThermoFisher Scientific, USA) for 2h at 55°C. After second strand synthesis (TargetAmp kit, EPICENTRE, USA), the DNA was fragmented using the Illumina Tagment DNA TDE1 Enzyme and Buffer Kits, which fragments DNA and inserts partial sequencing adapter sequences. Final PCR amplification of the libraries was done using KAPA HiFi HotStart Library Amplification Kit with unique dual indexing by IDT for Illumina Nextera DNA Unique Dual Indexes Sets. The barcoded libraries were purified and quantified using Qubit Fluorometric Quantification (ThermoFisher Scientific, USA). Size distribution of the library DNA was analyzed using the FragmentAnalyzer (Agilent,

172 USA). Sequencing of 2x150 bp was performed with NovaSeq sequencer (Illumina, USA)
173 according to the manufacturer's instructions, with a read depth of 20 million reads per sample.

174 2.3. Reduced representation bisulfite sequencing in brown adipose tissue

175 Genomic DNA from BAT samples were isolated using the DNeasy blood and tissue kit according
176 to the manufacturer's instructions (Qiagen, Hilden, Germany). Reduced representation bisulfite
177 sequencing (RRBS) library preparation was performed on 100 ng DNA using the Zymo-Seq RRBS
178 Library Kit (Zymo Research, Freiburg, Germany) by the core unit DNA-Technologien, Medical
179 Faculty Leipzig. Briefly, DNA was digested with 20U/µl MspI for 4h followed by RRBS adapter
180 ligation using 400U/µl T4 DNA ligase and gap filling with 2U/µl Taq DNA polymerase and 10mM
181 5-methylcytosine dNTP Mix. Bisulfite conversion was performed with lightning conversion
182 reagent, and the final samples were amplified using 5µM of the unique dual index Primer Set
183 (indexes 1-12) supplied by the manufacturer. Quality control was performed on the Bioanalyzer
184 (Illumina, USA) prior paired-end sequencing on the NovaSeq6000 platform (Illumina, USA) were
185 20 million reads per sample were obtained.

186 2.4. RNAseq data preprocessing

187 Raw RNAseq reads where quality-filtered and adapter-trimmed using Trimmomatic (v0.39) [14],
188 discarding reads shorter than 36 bp. Afterwards, reads were aligned to GRCm38.p6 reference
189 assembly using STAR (v2.7.8a) [15], allowing for a maximum of 50 multi-mapped reads. Gene
190 counts were quantified with featureCounts from the subread software package (v2.0.1) [16] with
191 multimappings counted by fractions.

192 2.5. Differential gene expression analysis

193 Transcripts without gene annotation and genes with a total count sum <10 were removed resulting
194 in 18k genes for subsequent gene expression analysis. Variance stabilization transformation (VST)
195 was applied to the filtered gene count matrix using the R package DESeq2 (v1.42.1) [17]. A
196 principal component analysis (PCA) was conducted to verify clustering of diet (HFD, chow) and
197 temperature (8°C, 30°C) groups within the gene expression signals. Three samples were identified
198 as outliers which did not cluster in their respective group according to the first two principal
199 components and were subsequently removed from the analysis. This resulted in group sizes of 7-8
200 mice reflecting all diet-temperature combinations ($N_{total} = 29$; $N_{HFD\_30°C} = 7$; $N_{HFD\_8°C} = 7$; $N_{chow\_30°C}$
201 $= 7$; $N_{chow\_8°C} = 8$). Afterwards, differential gene expression (DGE) analysis was performed with
202 DESeq2. Three comparisons were conducted: chow-fed mice at 8°C versus those at 30°C
203 ($COLD_{chow}$), HFD-fed mice at 8°C versus those at 30°C ($COLD_{HFD}$), and an interaction model
204 comparing $COLD_{HFD}$ versus $COLD_{chow}$ contrasts ($\Delta COLD_{diet}$). DEGs with a false discovery rate
205 (FDR) < 0.05 were considered statistically significant. DEG lists from each contrast where
206 subsequently matched with entries in the EpiFactors Database (v2.0,
207 https://epifactors.autosome.org, accessed on 10.09.2024) to investigate diet-specific methylation
208 regulators.

209 2.6. RBBS data processing

210 Raw RRBS reads from N = 29 mice ($N_{HFD\_30°C}$ = 7; $N_{HFD\_8°C}$ = 7; $N_{chow\_30°C}$ = 7; $N_{chow\_8°C}$ = 8) were
211 processed with the nextflow (v 23.04.3) [18] pipeline nf-core/methylseq (v2.4.0) [19] using the
212 parameters *--genome GRCm38 --non_directional --rrbs --skip_deduplication* and --
213 *cytosine_report*. In brief, quality filtering and adapter trimming of raw RRBS fastq files was
214 conducted with trimgalore (v0.6.7) [20] before running sequence alignments with Bismark
215 (v0.24.0) [21]. Afterwards, methylation signals are called with the Bismark methylation extractor
216 script including the build-in *coverage2cytosine* module for a genome-wide cytosine methylation
217 report which served as input for downstream analysis. Sex chromosomes were excluded.

218 2.7. Differential methylation analysis

219 To identify differentially methylated positions (DMPs) and differentially methylated regions
220 (DMRs), differential methylation analysis was conducted for $COLD_{chow}$, $COLD_{HFD}$, and
221 $\Delta COLD_{diet}$, utilizing beta values and the R packages limma (v3.54.0) [22] and RnBeads (v2.16.0)
222 [23] with parameters filtering.low.coverage.masking = TRUE, filtering.high.coverage.outliers =
223 TRUE and filtering.snp = "any". Based on their chromosomal position and respective annotation,
224 individual methylations can be contextualized within gene bodies or promoter regions (1500 bases
225 upstream and 500 bases downstream of the transcription start site), both of which were considered
226 in our analysis.

227 2.8. Integration of methylation and transcriptome data

228 After differential analysis of individual omics data, both gene expression and methylation signals
229 were combined to find biological associative effects between transcriptomics and epigenomics.
230 The R package biomaRt (v2.58.2) [24] was used to gather gene loci information for differentially
231 expressed genes (DEGs) and DMRs in gene and promotor context. Beta methylation values were
232 transformed to M-values using RnBeads. For each DEG, the corresponding DMR was selected
233 based on the alignment of gene IDs. M-values of all significantly DMPs overlapping with the DMR
234 were considered using the bedR (v1.0.7) [25] and the GenomicRanges (v1.54.1) [26] R packages.
235 Pearson correlation was then applied to find associations between DEG expression values and M-
236 values of each intersecting DMP using the multtest.cor function from RVAideMemoire (v0.9-83-
237 7) [27]. All DMPs with significant absolute Pearson correlations >0.5 between expression and
238 methylation signal ($p < 0.05$ without adjustment for multiple testing) were defined as differentially
239 methylated and expressed genes (DMEGs). If a DMEG is associated to both promoter and gene
240 body region, it was assigned to the DMR with the highest significance. This step was parallelized
241 with the foreach package (v1.5.2) [28]. The final list of DMEGs is comprised of genes with
242 significantly regulated expression signal (absolute $\log_2$ fold change (FC) >0.5) and methylation
243 signal (absolute $\log_2$ FC >1). Since several DMRs or DMPs can be differentially methylated within
244 a gene, several DMEGs were generated for such genes.

245 Subsequently, functional analysis of DMEGs was done with the use of QIAGEN Ingenuity
246 Pathway Analysis software (QIAGEN Inc., https://digitalinsights.qiagen.com/IPA, Winter Release
247 Q4 2024) [29] covering the catalog for disease and bio functions and canonical pathways. The
248 database query was limited within the IPA software to relationships with adipose tissue or
249 adipocytes in mice that are experimentally observed. Enrichments are reported with p after
250 Bonferroni-Holm (BH) adjustment and activation z-scores. Enrichments with BH corrected $p < 0.05$
251 are considered significant.

252 2.9. In vitro validation experiments

253 2.9.1. Immortalized and primary brown adipocytes

254 Immortalized (imBA [30]) and primary brown adipocytes were cultured and differentiated as
255 previously described [31]. At day 10, cells were harvested and subjected to further analyses.

256 2.9.2. In vitro manipulation of cellular DNA methylation levels

257 To analyze the effect of DNA methylation status on gene expression in imBA and primary brown
258 adipocytes, pre-adipocytes were treated with indicated concentrations of 5'aza-2'-deoxycytidine
259 (Aza) for 48h and subsequently differentiated [31]. Differentiated adipocytes at day 6 were treated
260 with indicated concentrations of S-adenosylmethionine (SAM, New England Biolabs) for 48h.
261 Differentiated adipocytes were harvested and subjected to further analysis.

262 2.9.3. Quantitative real-time-PCR (qPCR)

263 RNA from imBA and human primary SAT cells was isolated using RNeasy Lipid Tissue Mini kit.
264 qPCR was performed using the LightCycler System LC480 and LightCycler-DNA Master SYBR
265 Green I Kit (Roche, Mannheim, Germany). Adipocyte gene expression of candidate genes was
266 calculated by ΔΔCT method and normalized to *Nono* or *36b4* levels as indicated. Primer sequences
267 are listed in (Suppl. Table 1).

268 2.10. Statistical analysis

269 Analyses were performed under R version 4.3.2, except for mouse phenotyping data that was
270 analyzed using GraphPad Prism 10 (GraphPad, San Diego, CA, USA). Statistical tests are stated
271 in the figure legends. If not stated otherwise, adj. $p < 0.05$ were considered statistically significant.

272

3. Results

3.1. Phenotyping of chow and high fat diet-fed mice held at thermoneutrality or exposed to cold

Groups of 8 mice per diet were held at thermoneutrality (30°C) or in the cold (8°C) for 7 days (Figure 1A). Before the temperature challenge, mice were held at 23°C with HFD-fed mice presenting significantly higher body weights than chow fed mice (48.2 g vs 28.3 g, Figure 1B). In the cold, mice on chow diet maintained a steady body weight, while mice on HFD lost about 10% body weight (Figure 1B, C). All mice in the cold showed a significant drop in body temperature during the first days, but this loss in temperature was significantly higher in mice on HFD (-0.5°C vs -2°C after d1, Figure 1D). After 7 days, mice on chow diet recovered their body temperature to normal levels, while mice on HFD still had significantly lower temperatures (-1°C) (Figure 1D, E). Under thermoneutrality, mice on HFD had significantly higher BAT surface temperatures, consistent with increased diet-induced thermogenesis, but BAT surface temperatures were not different after cold exposure (Figure 1F, G). Extended phenotyping data is presented in Suppl. Figure 1.

3.2. Obesity impairs core transcriptome remodeling of BAT in response to cold

Gene expression data was used from all mice samples that also had methylation signal data available. After removal of outliers, N = 29 samples ($N_{HFD\_30°C}$ = 7; $N_{HFD\_8°C}$ = 7; $N_{chow\_30°C}$ = 7; $N_{chow\_8°C}$ = 8) remained for subsequent differential gene expression and methylation analysis. Analysis of VST normalized RNAseq expression counts shows clear clustering of all diet (chow, HFD)- and temperature (8°C, 30°C)-specific subgroups in the principal component analysis (Figure 2A), providing a solid basis for subsequent differential gene expression analysis. Moreover, temperature groups are separated by principal component 1 describing 33% of variance while diet groups are rather distinguished by principal component 2 covering 16,8% of total variance demonstrating an overall stronger impact of temperature compared to diet on overall gene expression patterns. Mice on HFD are older compared to chow fed mice. The age gap of 11 weeks could potentially interfere and explain a variance in the principal component analyses which was not addressed here.

To dissect BAT's physiological response to cold normal-weight control mice, we compared chow-fed mice held in the cold (8°C) with mice held at thermoneutrality (30°C) for one week. We will refer to this condition pair as $COLD_{chow}$. Additionally, to assess the effects of obesity on cold-induced BAT activation, we compared HFD-induced obese mice held in the cold (8°C) with mice held at thermoneutrality (30°C) for one week. This comparison will be referred to as $COLD_{HFD}$. Differential gene expression analysis (FDR <0.05) resulted in 7,089 DEGs for the $COLD_{chow}$ (Suppl. Figure 2A, B; Suppl. Table 2) and 5,249 DEGs for the $COLD_{HFD}$ (Suppl. Figure 2C, D; Suppl. Table 3) condition pairs. Reflecting the dominating effect of temperature on BAT activity, the majority of the significant DEGs overlap between the $COLD_{chow}$ and $COLD_{HFD}$ conditions are regulated similarly (N = 3,786; $COLD_{chow}$: 53%; $COLD_{HFD}$: 72%). Furthermore, 45% and 26% are

310 specifically regulated in $COLD_{chow}$ and $COLD_{HFD}$, respectively, while a total of 92 DEGs are
311 contrarily regulated (Suppl. Figure 4A).

312 To benchmark our $COLD_{chow}$ results with previously published data, we overlapped our DEGs with
313 those reported by Taylor et al. (2024) [32], who performed a comparable study in chow-fed male
314 mice exposed to severe cold (8 °C) versus thermoneutrality (28 °C) (Suppl. Figure 3; Suppl. Table
315 2). We found that 80% of our upregulated and 52% of our downregulated genes overlapped with
316 their DEGs, demonstrating a strong concordance across both directions in these independent
317 analyses.

318 Additionally, to investigate how diet affects BAT activation in response to cold exposure, we
319 employed an interaction model ($\Delta COLD_{diet}$) that compares the difference between both $COLD_{HFD}$
320 and $COLD_{chow}$ contrasts, rather than relying solely on simple group comparisons. This approach
321 enabled us to assess the combined and potentially synergistic or antagonistic effects of diet and
322 environment on BAT function [33]. Although an age gap of 11 weeks is indicated, mice on chow
323 or HFD are in a comparable age-range regarding BAT function and diet-independent body weight
324 development [34–37]. In total, we observed 1,364 genes (FDR <0.05) which are differentially
325 expressed between $COLD_{HFD}$ and $COLD_{chow}$ (Figure 2B, C; Suppl. Table 4). Since the most
326 significant DEGs are downregulated in the $COLD_{HFD}$ condition compared to $COLD_{chow}$, this
327 highlights a potential mechanism by which obesity may impair thermogenic capacity and energy
328 expenditure, suggesting that a high-fat diet disrupts the normal activation of BAT in response to
329 cold exposure.

330 3.3. Associations of gene expression and methylation signals underscore the influence of diet on
331 gene regulatory mechanisms

332 To explore the associative effects between transcriptomics and epigenomics, we correlated all
333 expression signals of DEGs with significant DMPs found within the DMRs of the corresponding
334 genes. This approach allowed us to define a set of differentially methylated and expressed genes
335 (DMEGs), using specific criteria: a Pearson correlation coefficient greater than ± 0.5, DEGs with
336 a $\log_2$ FC greater than ± 0.5 (adj. P <0.05), and DMPs with a $\log_2$ FC greater than ± 1 (p <0.05).
337 Importantly, we set a higher threshold for DMPs and focused on DMEGs located in both the
338 promoter and gene body regions, ensuring that our analysis captures the most relevant regulatory
339 elements influencing gene expression. To verify our findings, we analyzed the effect of DNA-
340 demethylation (using Aza) or hypermethylation (using SAM) on the expression of selected genes
341 in mouse adipocytes *in vitro* (Suppl. Figure 5). The observed effects of DNA methylation and the
342 manipulation on gene expression were in line with the results of our analysis correlating gene
343 expression and methylation and confirmed epigenetic control of gene expression in adipocytes.

344 In the $COLD_{chow}$ control comparison, we identified a total of 3,142 DMEGs among 21% (N =
345 1,524) of all DEGs. The data showed a balanced distribution of DMEGs, with 55% located within
346 gene bodies and 45% found in promoter regions (Figure 3A; Suppl. Table 5), indicating that
347 methylation can affect gene regulation through various mechanisms, such as promoter accessibility

348 or splice site manipulation. As illustrated in Figure 3B, DMEGs within the top 100 DMRs (ranked
349 by absolute $\log_2$ FC) are predominantly found in promoter regions and show distinctly higher
350 prevalence on chromosome 11.

351 To investigate which cell types might drive DNA methylation changes in BAT, we overlapped
352 DMEGs from the $COLD_{chow}$ condition with cell-type-specific marker genes derived from single-
353 cell RNAseq (scRNAseq) of BAT from male mice exposed to cold (5 °C) versus thermoneutrality
354 (30 °C) [38]. This analysis revealed that DMEGs were distributed across multiple cell types, with
355 the highest proportions in vascular smooth muscle cells (VSM, 43%), adipocytes (35%),
356 endothelial cells (EC, 31.8%), and stromal populations, including *Pdgfra*$^+$ adipocyte progenitor
357 cells (APCs, 28.1%) and pericytes (20.9%). In contrast, immune cells contributed more modestly,
358 with macrophages at 18.2%, NK cells at 9.3%, and T cell subsets (CD4$^+$, CD8$^+$, Treg) ranging from
359 5–9%. Across nearly all cell types, most DMEGs belonged to the hypo up category - genes
360 exhibiting hypomethylation accompanied by increased expression. This pattern was particularly
361 pronounced in adipocytes (26.4%) and vascular populations, including VSM (21.6%) and EC
362 (11.9%). Hyper up DMEGs were most notable in adipocytes (10%), whereas hypo down DMEGs
363 were enriched in vascular and stromal populations, including VSM (15%), EC (14.9%), *Pdgfra*$^+$
364 APCs (13.6%), and to a lesser extent in adipocytes (2.8%). Conversely, the fractions of hyper down
365 DMEGs were relatively small, ranging from 1-6% depending on the cell type (Figure 3C; Suppl.
366 Table 5).

367 Additionally, we detected 1,886 DMEGs from 19% (N = 1001) of all DGEs in the $COLD_{HFD}$
368 condition. Similar to the $COLD_{chow}$ condition, 60% of the DMEGs are located within gene bodies
369 and 40% in promoter regions (Figure 4A; Suppl. Table 6); however, the most highly regulated
370 DMEGs do not exhibit significant enrichment in the promoter regions (Figure 4B).

371 Although we previously observed that the majority of significant DEGs overlapping between the
372 $COLD_{chow}$ and $COLD_{HFD}$ conditions are regulated in a similar direction (Suppl. Figure 5), we
373 identified a contrasting pattern among the DMEGs. The gene expression of DMEGs shows
374 consistent regulatory patterns, with only 245 ($COLD_{chow}$: 16%; $COLD_{HFD}$: 24%) genes being
375 upregulated and 159 ($COLD_{chow}$: 10%; $COLD_{HFD}$: 16%) genes being downregulated in both
376 conditions (Suppl. Figure 4B; Suppl. Figure 6). In contrast, 73% and 60% are specifically regulated
377 in the $COLD_{chow}$ and $COLD_{HFD}$ conditions, respectively, while only one gene (*guanylyl cyclase*
378 *domain containing 1* (*Gucd1*)) is regulated in the opposite direction (Suppl. Figure 4B; Suppl.
379 Figure 7). This suggests that the response to temperature conditions is strongly dependent on the
380 specific environment and that methylation changes may be purposefully employed to adapt to
381 different metabolic or physiological demands.

382 Our previous findings revealed pronounced differences in the regulatory patterns of DMEGs
383 between the $COLD_{chow}$ and $COLD_{HFD}$ conditions by emphasizing the direction of regulation. To
384 further elucidate the nuances of diet-specific regulation, we utilized the $\Delta COLD_{diet}$ contrast to
385 detect more subtle differences in regulatory effects including regulation strength, directly

386 identifying diet-related differences in DMEGs associated with BAT activation induced by cold
387 exposure (Figure 5; Suppl. Table 7). For the $\Delta COLD_{diet}$ contrast, we detected 65 DMEGs from only
388 4% (N = 56) of all DEGs. Interestingly, these are primarily enriched in the gene bodies (69%),
389 suggesting that the regulation of these genes may be more influenced by post-transcriptional
390 mechanisms in response to cold exposure.

391 3.4. Adaptive divergence in thermogenic signaling reflects metabolic stress in obese BAT

392 For further characterization of the reported DMEGs, pathway enrichment analysis was performed
393 using the IPA software. The DMEGs were categorized into four groups: those exhibiting similar
394 regulation in both $COLD_{chow}$ and $COLD_{HFD}$ condition pairs, and those that are uniquely regulated
395 in each individual condition ($\Delta COLD_{diet,}$ $COLD_{chow}$, and $COLD_{HFD}$). Querying the catalog for
396 significant (BH-adjusted $p < 0.05$) canonical pathways (Figure 6; Suppl. Table 8) shows similar
397 activation of pathways with respect to lipid metabolism except for ketolysis which is only
398 significantly activated in the $COLD_{HFD}$ condition. Cell signaling and energy expenditure seem to
399 be activated or inhibited more differentially between $COLD_{chow}$ and $COLD_{HFD}$ condition pairs. For
400 example, the process of white adipose tissue browning is significantly inhibited in $COLD_{HFD}$ but
401 shows (unsignificant) activation in $COLD_{chow}$. Additionally, type II diabetes mellitus signaling is
402 significantly activated under $COLD_{HFD}$ considerations but tends to be (insignificantly) inhibited
403 under $COLD_{chow}$.

404 3.5. Diet and cold exposure shape epigenetic regulation in BAT

405 To gain deeper insights into the epigenetic mechanisms that regulate BAT activation and
406 thermogenesis under different dietary conditions, we matched DEGs from each condition pair with
407 the EpiFactors database (v2.0, https://epifactors.autosome.org, accessed on 10.09.2024), with the
408 analysis being restricted to DNA-methylation-related factors, while histone-modifying enzymes,
409 chromatin remodelers and RNA-based epigenetic regulators were omitted. As summarized in
410 Figure 7, we identified eleven differentially expressed methylation regulators for the $COLD_{chow}$,
411 seven for $COLD_{HFD}$, and four for $\Delta COLD_{diet}$ condition pairs. Notably, five regulators were found
412 to be common to both the $COLD_{chow}$ and $COLD_{HFD}$ conditions including *Tet2* (*ten-eleven*
413 *translocation methylase 2*), *Dnmt3* (*DNA methyltransferase 3*), *Cenpc1* (*centromere protein C*),
414 *Apobec1* (*apolipoprotein B mRNA editing enzyme catalytic subunit 1*) which are all downregulated
415 in $COLD_{chow}$ *and* $COLD_{HFD}$. This overlap indicates a conserved epigenetic mechanism that is
416 essential for the physiological response to cold exposure, regardless of diet. However, the majority
417 of methylation enzymes exhibited unique regulation within each condition pair, highlighting the
418 nuanced regulation of epigenetic mechanisms based on dietary composition. For instance, *Tet3* and
419 *Dnmt1* were differently regulated within the $\Delta COLD_{diet}$ and $COLD_{chow}$ conditions, while *Mettl4*
420 (*methyltransferase-like protein 4*) and *Apobec3b* showed differential regulation within the
421 $\Delta COLD_{diet}$ contrast.

422

4. Discussion

We aimed to explore how environmental factors and DNA methylation may influence BAT function. To investigate potential links between DNA methylation and gene expression, we integrated RNA-seq data with RRBS methylation profiles to identify genes with coordinated changes in expression and methylation (DMEGs) under different dietary and thermal conditions. This approach provides insights into BAT plasticity and adaptive thermogenesis, contributing to a foundational understanding that could inform future obesity-related research and interventions.

Consistent with BAT's physiological adaptation to cold, our data show that cold exposure robustly increases BAT activity regardless of diet, evidenced by strong transcriptomic responses with 7,089 DEGs in chow-fed and 5,249 DEGs in HFD-fed mice. A substantial overlap (~3,780 genes) between both dietary groups suggests a conserved "core" thermogenic program that remains inducible under obesogenic conditions. Notably, *Ucp1*, a central mediator of non-shivering thermogenesis, and *Letmd1* (*leucine zipper-EF-hand-containing transmembrane protein domain containing 1*), which is essential for mitochondrial integrity and cold response, were among the top upregulated genes across both diets. Their consistent induction under cold exposure, aligns with previous reports of diet-insensitive thermogenic regulators [39,40]. Beside this shared response, ~1,360 genes were differentially expressed between the cold-exposed groups ($\Delta COLD_{diet}$), with most downregulated in diet-induced obese mice, consistent with a high-fat diet impairing thermoregulatory capacity driven by mitochondrial dysfunction, inflammation, and insulin resistance [41,42]. This functional attenuation under high-fat diet conditions is also reflected among the most strongly regulated DGEs. Downregulation of *Hk2* (*hexokinase 2*), a key glycolytic enzyme, has been linked to reduced glucose uptake [43]. Similarly, reduced *Gpd1* (*glycerol-3-phosphate dehydrogenase 1*) expression, part of the glycerol-3-phosphate shuttle, may reflect compromised lipid metabolism. *Ucp1* stayed cold-inducible in all diets but was lower in HFD-fed mice, showing that thermogenic response is maintained but reduced under metabolic stress. This aligns with reports of reduced BAT activity in obesity despite retained gene expression [39]. Our results of $COLD_{chow}$ are in line with those of Taylor et al. (2024) [32], who performed a comparable study in chow-fed mice exposed to severe cold (8°C) versus thermoneutrality (28°C). The strong overlap of DEGs highlights the reproducibility of cold-induced BAT transcriptional responses across independent studies and supports the generalizability of our findings.

To identify epigenetically regulated genes, we correlated methylation changes (M-values of DMPs overlapping DMRs) with gene expression levels to define DMEGs. While these correlations suggest potential regulatory links, they do not establish causality, as gene expression is also influenced by other epigenetic modifications and transcription factors [32,44,45]. More comprehensive approaches integrating histone modifications, proteomics, or single-cell epigenomics could further elucidate the complex regulation within heterogeneous BAT cell populations [46]. Compared to generalized linear models with distributional assumptions [47,48], our site-specific correlation approach offers higher sensitivity for detecting local methylation-expression relationships, though it may miss broader regulatory patterns and is more sensitive to

462 noise. Our thresholds for defining significant DMEGs were set at |log FC| >0.5 for expression
463 changes and |log FC| >1 for methylation differences; correlations were considered significant if |r|
464 >0.5 and p <0.05. These cutoffs balance sensitivity and specificity but also limit detection power
465 given our sample size. When DMEGs overlapped promoter and gene body regions, assignment
466 was based on the strongest correlation, which enhances interpretability but may introduce bias due
467 to regional variability or technical factors.

468 By analyzing DMEGs, ~3,100 DMEGs (21% of DGEs) were identified in $COLD_{chow}$, with a
469 roughly equal distribution between promoter and gene body methylation. In contrast, HFD-fed
470 mice exhibited only ~1,900 DMEGs (19% of DEGs), with a higher proportion of gene body
471 methylation. As gene body methylation is often linked to transcript fine-tuning rather than
472 activation, this may reflect constrained thermogenic adaptability under obesogenic conditions [49].
473 Notably, DMEGs were largely condition-specific despite substantial overlap in DEGs, highlighting
474 that diet and cold exposure interact to shape BAT-specific regulatory states, rather than acting
475 independently. These condition-specific methylation-expression relationships suggest that DNA
476 methylation may play an active role in modulating transcriptional plasticity and energy
477 metabolism, enabling BAT to adapt epigenetically to distinct environmental challenges.

478 To gain further insight into the cellular context of these DNA methylation changes, we mapped
479 DMEGs of the $COLD_{chow}$ condition onto cell-type-specific markers derived from male mice
480 scRNAseq data of cold-exposed BAT [38]. This analysis revealed that the majority of DMEGs
481 belonged to the hypo up category, particularly in adipocytes, vascular cells, and *Pdgfra*$^{+}$ adipocyte
482 progenitors, suggesting coordinated activation of thermogenic programs and vascular remodeling.
483 Hypo down DMEGs were enriched in vascular and stromal populations, indicating selective
484 repression of pathways supporting tissue structure and function. Hyper up DMEGs were primarily
485 observed in adipocytes, whereas hyper down DMEGs were rare (1–6%), implying that DNA
486 methylation mediated silencing plays a limited role in the cold response. The observed cell type-
487 specific DMEG distributions are consistent with prior evidence of increased intercellular signaling
488 among adipocytes, vascular, stromal, and immune cells under cold conditions in chow-fed mice,
489 suggesting an epigenetic basis for the transcriptional remodeling in BAT [38].

490 Pathway enrichment analysis further supports this adaptive divergence of DMEGs and highlighting
491 the diet-dependent rewiring of thermogenic signaling. Cold exposure activated distinct lipid
492 metabolic pathways (triacylglycerol, phosphatidylglycerol, and CDP−diacylglycerol biosynthesis)
493 in both dietary groups, however, ketolysis was selectively enriched in HFD-fed mice. In line with
494 previous findings that HFD suppresses ketone body utilization for lipogenesis in BAT via
495 downregulation of *acetoacetyl-CoA synthetase* (*Aacs*) [50], our DGE analysis show that *Aacs* was
496 significantly upregulated by cold in both dietary groups, but this response was markedly stronger
497 in chow-fed mice ($\log_2$ FC: 1.77) than in HFD-fed mice ($\log_2$ FC: 0.74), with a negative interaction
498 effect ($\Delta COLD_{diet}$ l $\log_2$ FC: –0.81). These results indicate that cold-induced ketone body recycling
499 remains inducible but is dampened under HFD, potentially limiting metabolic flexibility and
500 compensatory lipid synthesis in insulin-resistant BAT. Consistently, only $COLD_{HFD}$ showed

activation of the Type II Diabetes Mellitus signaling pathway under cold stress, reflecting a diabetogenic transcriptional environment marked by insulin resistance and impaired glucose homeostasis [51]. This suggests that cold exposure does not fully overcome metabolic dysfunction in BAT during obesity, potentially limiting its systemic metabolic benefits.

Further, cold-exposed HFD mice uniquely activated Sirtuin signaling, potentially a compensatory response to mitochondrial stress, while suppressing pathways related to mitochondrial dysfunction and white adipose tissue browning, indicating a shift from efficient thermogenesis to cellular maintenance [52]. Further, a selective activation of neuroendocrine pathways (e.g., corticotropin-releasing hormone and orexin signaling) may reflect rewiring of central and peripheral regulatory mechanisms to compensate for reduced intrinsic thermogenic capacity [53]. Concurrent suppression of nitric oxide and neuronal nitric oxide synthase (nNOS) signaling, crucial for vascular perfusion and mitochondrial function, points to impaired BAT structural and vascular adaptation under HFD.

We identified several epigenetic regulators differentially expressed in response to cold and diet. Core factors such as *Tet2*, *Dnmt3*, *Cenpc1*, and *Apobec1* responded similarly under both diets, suggesting a foundational epigenetic program supporting cold-induced chromatin remodeling and transcriptomic flexibility. In contrast to white adipose tissue, where *Mettl4* is upregulated under obesogenic conditions [54], we observed its downregulation in BAT only in $COLD_{HFD}$. Given that Mettl4-mediated N6-adenine methylation has been implicated in adipocyte differentiation and lipid production [55], it is conceivable that high-fat diets constrain the differentiation and functional capacity of BAT through epigenetic mechanisms. Conversely, cold exposure decreased *Tet3* and *Dnmt1* expression under chow but not HFD. As Tet3 and Dnmt1 regulate adipocyte expansion and mitochondrial function as well as chromatin architecture, respectively, their cold-induced downregulation may favor thermogenesis by limiting hypertrophy and enhancing mitochondrial and epigenetic adaptability [56–58]. *Dnmt1* deletion in BAT has no metabolic impact under standard diets [59], but may gain relevance under thermogenic or obesogenic stress. A previous study demonstrated the downregulation of *Dnmt1*, *Dnmt3a,* and *Dnmt3b* in BAT upon cold exposure under chow diet conditions, linking reduced DNA methylation to enhanced thermogenic activation [60]. Our findings confirm this pattern under chow conditions but reveal a lack of regulation under HFD, supporting the notion that epigenetic flexibility is impaired in obesogenic environments. *Apobec3*, a cytidine deaminase implicated in RNA and potentially DNA editing [61], was downregulated by cold under both diets, though significantly more under chow. This pattern may reflect its role in facilitating transcriptomic remodeling during thermogenic activation that may be blunted under HFD. Therefore, BAT activation appears to be governed by a conserved core of methylation regulators responsive to cold, while additional, context-specific pathways are modulated by the dietary environment. This dual mechanism supports a model in which a stable epigenetic framework is dynamically adjusted to accommodate metabolic demands, thereby fine-tuning the thermogenic capacity of BAT.

By conducting in vitro methylation analyses, we confirmed the epigenetic transcription control of certain DMEGs and important BAT regulatory genes such as *Bmp8b* or *Cpne5* pointing towards a valid impact of the DNA methylation on BAT function. By using Aza and SAM, we cannot rule out the possibility that other epigenetic mechanisms than DNA methylation led to these observations as especially SAM serves as methyldonor for various processes [62]. In any case, our results strongly support the highly dynamic control of BAT by epigenetic alterations.

4.1. Limitations

A limitation arises from age differences between diet groups (11 weeks chow vs. 22 weeks HFD). First, the difference in bodyweight between chow and HFD mice may have partially arisen from the age gap, as there is still a slow increase in body weight beyond adulthood at 12 weeks of age [37]. However, male chow fed mice at 22 weeks of age would reach approximately 30g bodyweight which still is significantly different from mice on HFD at the same age. Second, although BAT function declines with age, mice used in this study are of a comparable age-range related to BAT function. Studies show that mice aged between 12 weeks and six months present a stable metabolic active BAT, with stable mitochondrial content and thermogenic potential before these factors start to decline and lipid accumulation increases [34–36]. Although we cannot bioinformatically address this issue in our comparative analyses, we believe that age is not a main driving factor of the here observed effects as we addressed a comparable age range regarding bodyweight and cold adaptation of BAT. Anyway, regardless of BAT function, global DNA methylation reduces with age while specifically promoter regions tend to get hypermethylated with age [63]. While we cannot address the age factor in our analyses due to group specific age differences, we expect a limited impact of age on our results based on comparing mice in a suitable age range meaning only "young adult mice" [64]. A further limitation is the use of only male mice, which may limit generalizability to females. However, given the known sex-specific differences in adipose biology, BAT activity, and epigenetic regulation, addressing only males is beneficial regarding the addressed methodology. Future studies should include female mice to assess potential sex-by-diet or sex-by-temperature interactions. Small sample sizes (7-8 per group) limit statistical power to detect subtle effects. In addition, RRBS data provides only partial genome coverage, primarily focusing on CpG-rich regions, potentially overlooking important regulatory areas outside these regions. In contrast, whole-genome bisulfite sequencing could provide more comprehensive methylation profiling.

5. Conclusions

In conclusion, this study provides the first evidence that cold-induced DNA methylation remodeling in BAT is strongly shaped by dietary context, particularly under obesogenic conditions. Our integrative analysis reveals that, while cold exposure activates a conserved thermogenic transcriptional program, high-fat diet attenuates epigenetic flexibility and restricts full BAT activation. These findings underscore that environmental temperature and dietary intake interact to regulate BAT function via interconnected transcriptional and epigenetic mechanisms. Importantly,

577 we identify both core and context-specific regulators that mediate this response, offering potential
578 molecular targets for future therapies. By demonstrating that obesity alters the epigenetic landscape
579 of cold adaptation, our study opens new avenues for nutritional or epigenetic interventions aimed
580 at restoring BAT plasticity and enhancing thermogenic capacity in metabolic disease.

581 **Data Availability**

582 Raw RNAseq and RRBS data have been deposited in the Sequence Read Archive (SRA,
583 https://www.ncbi.nlm.nih.gov/sra/) [65] under the BioProject number PRJNA1294891.

584 **Acknowledgements**

585 We acknowledge the technical support of the Core Unit DNA Technologies of the Faculty of
586 Medicine, University of Leipzig, and thank Dr. Knut Krohn, Stefanie Ziesche and Kathleen Schön.
587 We thank Jenny Schuster and Lisa Gärtner from the animal facility, and Ines Müller, Claudia
588 Gebhardt and Olivia Paetow for excellent technical assistance.

589 **Author contributions**

590 Conceptualization: TH, AH, KRZ, JTH, and JW; Methodology: AH, TH, KRZ, and JW;
591 Investigation: KRZ, HB, and JW; Validation: KRZ, HB, and JW; Formal analysis: TH; Data
592 curation: TH and AH; Writing – original draft: TH, AH, KRZ, JW, and JTH; Writing – review &
593 editing: TH, AH, KRZ, HB, LM, PK, MS, MB, JTH, and JW; Visualization: TH; Supervision: AH
594 and JTH; Funding acquisition: MB, JW, and JTH.

595 **Funding**

596 This work was funded or supported by grants of the Deutsche Forschungsgemeinschaft, project
597 number 209933838 (SFB1052 "Obesity Mechanisms": B1 to MB, C7 to JTH) and by the Formel1
598 Nachwuchsförderung of the Medical Faculty of the University of Leipzig (JW). HB is supported
599 by a doctoral scholarship of the Studienstiftung des Deutschen Volkes. LM is supported by
600 the Swedish Research Council, the European for the Study of Diabetes and the German Diabetes
601 Association.

602 **Conflict of interest**

603 MB received honoraria as a consultant and speaker from Amgen, AstraZeneca, Bayer, Boehringer-
604 Ingelheim, Lilly, Novo Nordisk, Novartis, and Sanofi. All other authors declare no conflicts of
605 interest. The funders had no role in the design of the study, the collection, analyses, or interpretation
606 of data, in the decision to publish the results and the writing of the manuscript.

607

608

609 **References**

610 [1] Kusminski CM, Bickel PE, Scherer PE. Targeting adipose tissue in the treatment of
611 obesity-associated diabetes. Nat Rev Drug Discov 2016;15:639–60.
612 https://doi.org/10.1038/nrd.2016.75.
613 [2] Saito M, Matsushita M, Yoneshiro T, Okamatsu-Ogura Y. Brown Adipose Tissue, Diet-
614 Induced Thermogenesis, and Thermogenic Food Ingredients: From Mice to Men. Front
615 Endocrinol 2020;11. https://doi.org/10.3389/fendo.2020.00222.
616 [3] U Din M, Saari T, Raiko J, Kudomi N, Maurer SF, Lahesmaa M, et al. Postprandial
617 Oxidative Metabolism of Human Brown Fat Indicates Thermogenesis. Cell Metab 2018;28:207-
618 216.e3. https://doi.org/10.1016/j.cmet.2018.05.020.
619 [4] Chouchani ET, Kazak L, Spiegelman BM. New Advances in Adaptive Thermogenesis:
620 UCP1 and Beyond. Cell Metab 2019;29:27–37. https://doi.org/10.1016/j.cmet.2018.11.002.
621 [5] Rosenbaum M, Leibel RL. Adaptive thermogenesis in humans. Int J Obes 2010;34:S47–
622 55. https://doi.org/10.1038/ijo.2010.184.
623 [6] Scheele C, Wolfrum C. Brown Adipose Crosstalk in Tissue Plasticity and Human
624 Metabolism. Endocr Rev 2020;41:53–65. https://doi.org/10.1210/endrev/bnz007.
625 [7] Xiao H, Kang S. The role of DNA methylation in thermogenic adipose biology.
626 Epigenetics 2019;14:837–43. https://doi.org/10.1080/15592294.2019.1625670.
627 [8] Wang S, Cao Q, Cui X, Jing J, Li F, Shi H, et al. Dnmt3b Deficiency in Myf5+-Brown
628 Fat Precursor Cells Promotes Obesity in Female Mice. Biomolecules 2021;11:1087.
629 https://doi.org/10.3390/biom11081087.
630 [9] Teperino R. Intergenerational metabolic effects of cold exposure. Nat Metab 2025;7:635–
631 6. https://doi.org/10.1038/s42255-025-01222-z.
632 [10] Sun S, Hood M, Scott L, Peng Q, Mukherjee S, Tung J, et al. Differential expression
633 analysis for RNAseq using Poisson mixed models. Nucleic Acids Res 2017;45:e106–e106.
634 https://doi.org/10.1093/nar/gkx204.
635 [11] Skinner MK. Preconception cold–induced epigenetic inheritance. Nat Med
636 2018;24:1308–9. https://doi.org/10.1038/s41591-018-0187-3.
637 [12] Zhang Q, Xiao X, Zheng J, Li M, Yu M, Ping F, et al. Maternal High-Fat Diet Disturbs
638 the DNA Methylation Profile in the Brown Adipose Tissue of Offspring Mice. Front Endocrinol
639 2021;12. https://doi.org/10.3389/fendo.2021.705827.
640 [13] Madden CJ, Morrison SF. A high-fat diet impairs cooling-evoked brown adipose tissue
641 activation via a vagal afferent mechanism. Am J Physiol-Endocrinol Metab 2016;311:E287–92.
642 https://doi.org/10.1152/ajpendo.00081.2016.
643 [14] Bolger AM, Lohse M, Usadel B. Trimmomatic: a flexible trimmer for Illumina sequence
644 data. Bioinforma Oxf Engl 2014;30:2114–20. https://doi.org/10.1093/bioinformatics/btu170.
645 [15] Dobin A, Davis CA, Schlesinger F, Drenkow J, Zaleski C, Jha S, et al. STAR: ultrafast
646 universal RNA-seq aligner. Bioinforma Oxf Engl 2013;29:15–21.
647 https://doi.org/10.1093/bioinformatics/bts635.
648 [16] Liao Y, Smyth GK, Shi W. featureCounts: an efficient general purpose program for
649 assigning sequence reads to genomic features. Bioinforma Oxf Engl 2014;30:923–30.
650 https://doi.org/10.1093/bioinformatics/btt656.
651 [17] Love MI, Huber W, Anders S. Moderated estimation of fold change and dispersion for
652 RNA-seq data with DESeq2. Genome Biol 2014;15:1–21. https://doi.org/10.1186/s13059-014-
653 0550-8.
654 [18] Di Tommaso P, Chatzou M, Floden EW, Barja PP, Palumbo E, Notredame C. Nextflow
655 enables reproducible computational workflows. Nat Biotechnol 2017;35:316–9.

656 https://doi.org/10.1038/nbt.3820.
657 [19] Ewels P, Hammarén R, Peltzer A, phue, F S, Tommaso PD, et al. nf-core/methylseq 2019.
658 https://doi.org/10.5281/zenodo.2555454.
659 [20] Martin M. Cutadapt removes adapter sequences from high-throughput sequencing reads.
660 EMBnetJournal 2011;17:10–2. https://doi.org/10.14806/ej.17.1.200.
661 [21] Krueger F, Andrews SR. Bismark: a flexible aligner and methylation caller for Bisulfite-
662 Seq applications. Bioinformatics 2011;27:1571–2. https://doi.org/10.1093/bioinformatics/btr167.
663 [22] Ritchie ME, Phipson B, Wu D, Hu Y, Law CW, Shi W, et al. limma powers differential
664 expression analyses for RNA-sequencing and microarray studies. Nucleic Acids Res
665 2015;43:e47. https://doi.org/10.1093/nar/gkv007.
666 [23] Müller F, Scherer M, Assenov Y, Lutsik P, Walter J, Lengauer T, et al. RnBeads 2.0:
667 comprehensive analysis of DNA methylation data. Genome Biol 2019;20:55.
668 https://doi.org/10.1186/s13059-019-1664-9.
669 [24] Durinck S, Moreau Y, Kasprzyk A, Davis S, De Moor B, Brazma A, et al. BioMart and
670 Bioconductor: a powerful link between biological databases and microarray data analysis.
671 Bioinformatics 2005;21:3439–40. https://doi.org/10.1093/bioinformatics/bti525.
672 [25] Haider S, Waggott D, Boutros P. bedr: Genomic Region Processing using Tools Such as
673 'BEDTools','BEDOPS'and 'Tabix' 2019.
674 [26] Lawrence M, Huber W, Pagès H, Aboyoun P, Carlson M, Gentleman R, et al. Software
675 for Computing and Annotating Genomic Ranges. PLoS Comput Biol 2013;9.
676 https://doi.org/10.1371/journal.pcbi.1003118.
677 [27] HERVE M. RVAideMemoire: Testing and Plotting Procedures for Biostatistics. 2023.
678 [28] Microsoft, Weston S. foreach: Provides Foreach Looping Construct. 2022.
679 [29] Krämer A, Green J, Pollard J, Tugendreich S. Causal analysis approaches in Ingenuity
680 Pathway Analysis. Bioinformatics 2014;30:523–30.
681 https://doi.org/10.1093/bioinformatics/btt703.
682 [30] Klein J, Fasshauer M, Klein HH, Benito M, Kahn CR. Novel adipocyte lines from brown
683 fat: A model system for the study of differentiation, energy metabolism, and insulin action.
684 BioEssays 2002;24:382–8. https://doi.org/10.1002/bies.10058.
685 [31] Weiner J, Rohde K, Krause K, Zieger K, Klöting N, Kralisch S, et al. Brown adipose
686 tissue (BAT) specific vaspin expression is increased after obesogenic diets and cold exposure and
687 linked to acute changes in DNA-methylation. Mol Metab 2017;6:482–93.
688 https://doi.org/10.1016/j.molmet.2017.03.004.
689 [32] Taylor BC, Steinthal LH, Dias M, Yalamanchili HK, Ochsner SA, Zapata GE, et al.
690 Histone proteoform analysis reveals epigenetic changes in adult mouse brown adipose tissue in
691 response to cold stress. Epigenetics Chromatin 2024;17. https://doi.org/10.1186/s13072-024-
692 00536-8.
693 [33] Nedergaard J, Cannon B. The browning of white adipose tissue: some burning issues. Cell
694 Metab 2014;20:396–407. https://doi.org/10.1016/j.cmet.2014.07.005.
695 [34] Cannon B, De Jong JMA, Fischer AW, Nedergaard J, Petrovic N. Human brown adipose
696 tissue: Classical brown rather than brite/beige? Exp Physiol 2020;105:1191–200.
697 https://doi.org/10.1113/EP087875.
698 [35] Silva GDN, Amato AA. Thermogenic adipose tissue aging: Mechanisms and
699 implications. Front Cell Dev Biol 2022;10:955612. https://doi.org/10.3389/fcell.2022.955612.
700 [36] Zoico E, Rubele S, De Caro A, Nori N, Mazzali G, Fantin F, et al. Brown and Beige
701 Adipose Tissue and Aging. Front Endocrinol 2019;10:368.
702 https://doi.org/10.3389/fendo.2019.00368.
703 [37] The Jackson Laboratory. Body Weight Information for B6J (000664) 2025.

704 https://www.jax.org/jax-mice-and-services/strain-data-sheet-pages/body-weight-chart-000664.
705 [38] Shamsi F, Zheng R, Ho L-L, Chen K, Tseng Y-H. Comprehensive analysis of
706 intercellular communication in the thermogenic adipose niche. Commun Biol 2023;6:761.
707 https://doi.org/10.1038/s42003-023-05140-2.
708 [39] Fromme T, Klingenspor M. Uncoupling protein 1 expression and high-fat diets. Am J
709 Physiol-Regul Integr Comp Physiol 2011;300:R1–8. https://doi.org/10.1152/ajpregu.00411.2010.
710 [40] Choi K-M, Kim JH, Kong X, Isik M, Zhang J, Lim H-W, et al. Defective brown adipose
711 tissue thermogenesis and impaired glucose metabolism in mice lacking Letmd1. Cell Rep
712 2021;37:110104. https://doi.org/10.1016/j.celrep.2021.110104.
713 [41] Bournat JC, Brown CW. Mitochondrial dysfunction in obesity. Curr Opin Endocrinol
714 Diabetes Obes 2010;17:446–52. https://doi.org/10.1097/MED.0b013e32833c3026.
715 [42] Maliszewska K, Kretowski A. Brown Adipose Tissue and Its Role in Insulin and Glucose
716 Homeostasis. Int J Mol Sci 2021;22:1530. https://doi.org/10.3390/ijms22041530.
717 [43] Shimobayashi M, Thomas A, Shetty S, Frei IC, Wölnerhanssen BK, Weissenberger D, et
718 al. Diet-induced loss of adipose hexokinase 2 correlates with hyperglycemia. eLife
719 2023;12:e85103. https://doi.org/10.7554/eLife.85103.
720 [44] Kouzarides T. Chromatin Modifications and Their Function. Cell 2007;128:693–705.
721 https://doi.org/10.1016/j.cell.2007.02.005.
722 [45] Lee TI, Young RA. Transcriptional regulation and its misregulation in disease. Cell
723 2013;152:1237–51. https://doi.org/10.1016/j.cell.2013.02.014.
724 [46] Smallwood SA, Lee HJ, Angermueller C, Krueger F, Saadeh H, Peat J, et al. Single-cell
725 genome-wide bisulfite sequencing for assessing epigenetic heterogeneity. Nat Methods
726 2014;11:817–20. https://doi.org/10.1038/nmeth.3035.
727 [47] Gevaert O, Tibshirani R, Plevritis SK. Pancancer analysis of DNA methylation-driven
728 genes using MethylMix. Genome Biol 2015;16:17. https://doi.org/10.1186/s13059-014-0579-8.
729 [48] Mishra NK, Guda C. Genome-wide DNA methylation analysis reveals molecular
730 subtypes of pancreatic cancer. Oncotarget 2017;8:28990–9012.
731 https://doi.org/10.18632/oncotarget.15993.
732 [49] Moore LD, Le T, Fan G. DNA Methylation and Its Basic Function.
733 Neuropsychopharmacology 2013;38:23–38. https://doi.org/10.1038/npp.2012.112.
734 [50] Yamasaki M, Hasegawa S, Ozaki S, Imai M, Saito D, Takahashi N. High-Fat-Diet
735 Suppressed Ketone Body Utilization for Lipogenic Pathway in Brown Adipose Tissues.
736 Metabolites 2023;13:519. https://doi.org/10.3390/metabo13040519.
737 [51] Chondronikola M, Volpi E, Børsheim E, Porter C, Saraf MK, Annamalai P, et al. Brown
738 Adipose Tissue Activation Is Linked to Distinct Systemic Effects on Lipid Metabolism in
739 Humans. Cell Metab 2016;23:1200–6. https://doi.org/10.1016/j.cmet.2016.04.029.
740 [52] Escalona-Garrido C, Vázquez P, Mera P, Zagmutt S, García-Casarrubios E, Montero-
741 Pedrazuela A, et al. Moderate SIRT1 overexpression protects against brown adipose tissue
742 inflammation. Mol Metab 2020;42:101097. https://doi.org/10.1016/j.molmet.2020.101097.
743 [53] Madden CJ, Tupone D, Morrison SF. Orexin modulates brown adipose tissue
744 thermogenesis. Biomol Concepts 2012;3:381–6. https://doi.org/10.1515/bmc-2011-0066.
745 [54] Kang Q, Zhu X, Ren D, Ky A, MacDougald OA, O'Rourke RW, et al. Adipose
746 METTL14-Elicited N^6-Methyladenosine Promotes Obesity, Insulin Resistance, and NAFLD
747 Through Suppressing β Adrenergic Signaling and Lipolysis. Adv Sci 2023;10.
748 https://doi.org/10.1002/advs.202301645.
749 [55] Zhang Z, Hou Y, Wang Y, Gao T, Ma Z, Yang Y, et al. Regulation of Adipocyte
750 Differentiation by METTL4, a 6 mA Methylase. Sci Rep 2020;10.
751 https://doi.org/10.1038/s41598-020-64873-w.

752 [56] Jung BC, You D, Lee I, Li D, Schill RL, Ma K, et al. TET3 plays a critical role in white
753 adipose development and diet-induced remodeling. Cell Rep 2023;42:113196.
754 https://doi.org/10.1016/j.celrep.2023.113196.
755 [57] Park J, Lee DH, Ham S, Oh J, Noh J-R, Lee YK, et al. Targeted erasure of DNA
756 methylation by TET3 drives adipogenic reprogramming and differentiation. Nat Metab
757 2022;4:918–31. https://doi.org/10.1038/s42255-022-00597-7.
758 [58] Kajimura S. The epigenetic regulation of adipose tissue plasticity. Proc Natl Acad Sci
759 2021;118. https://doi.org/10.1073/pnas.2102944118.
760 [59] Park YJ, Lee S, Lim S, Nahmgoong H, Ji Y, Huh JY, et al. DNMT1 maintains metabolic
761 fitness of adipocytes through acting as an epigenetic safeguard of mitochondrial dynamics. Proc
762 Natl Acad Sci 2021;118. https://doi.org/10.1073/pnas.2021073118.
763 [60] Taylor BC, Steinthal LH, Dias M, Yalamanchili HK, Ochsner SA, Zapata GE, et al.
764 Histone proteoform analysis reveals epigenetic changes in adult mouse brown adipose tissue in
765 response to cold stress. Epigenetics Chromatin 2024;17:12. https://doi.org/10.1186/s13072-024-
766 00536-8.
767 [61] Silvas TV, Schiffer CA. APOBEC3s: DNA-editing human cytidine deaminases. Protein
768 Sci Publ Protein Soc 2019;28:1552–66. https://doi.org/10.1002/pro.3670.
769 [62] Schmidt T. S-Adenosylmethionine affects ERK1/2 and STAT3 pathway in androgen-
770 independent prostate cancer cells. Mol Biol Rep 2022;49:4805–17.
771 https://doi.org/10.1007/s11033-022-07331-2.
772 [63] Perez-Correa J-F, Tharmapalan V, Geiger H, Wagner W. Epigenetic Clocks for Mice
773 Based on Age-Associated Regions That are Conserved Between Mouse Strains and Human.
774 Front Cell Dev Biol 2022;10:902857. https://doi.org/10.3389/fcell.2022.902857.
775 [64] Berry DC, Stenesen D, Zeve D, Graff JM. The developmental origins of adipose tissue.
776 Development 2013;140:3939–49. https://doi.org/10.1242/dev.080549.
777 [65] Katz K, Shutov O, Lapoint R, Kimelman M, Brister JR, O'Sullivan C. The Sequence
778 Read Archive: a decade more of explosive growth. Nucleic Acids Res 2022;50:D387–90.
779 https://doi.org/10.1093/nar/gkab1053.
780

781 **Figure legends**

782 **Figure 1: Phenotyping of chow and HFD-fed mice housed at 30°C or 8°C.** (A) Schematic
783 overview and corresponding color code of the cohort mouse groups stratified by dietary (chow,
784 HFD) and environmental (thermoneutrality vs cold) conditions. (B) Body weight development and
785 (C) body weight change in chow and HFD-fed mice housed at thermoneutrality (30°C) or in the
786 cold (8°C) for 7 days. Body temperature (D) and temperature change (E) in chow and HFD-fed
787 mice housed at thermoneutrality (30°C) or in the cold (8°C) for 7 days. (F) Thermal images from
788 brown adipose tissue (BAT) and (G) BAT surface temperature in chow and HFD-fed mice housed
789 at thermoneutrality (30°C) or in the cold (8°C) for 7 days. N = 7-8 per condition. (B, D) Statistical
790 significance was evaluated by two-way ANOVA with uncorrected Fischer's LSD, (E) Šídák's post-
791 hoc test, (C, G) or one-way ANOVA with Tukey's post-hoc test. $p < 0.05$ (*), $p < 0.01$ (**), $p < 0.001$
792 (***). Scale bar: 100 µm.

793 **Figure 2: RNA sequencing-based gene expression data revealse distinct clusters of treatment**
794 **groups.** (A) Principal component analysis separates temperature and diet. All considered
795 subgroups reveal distinct expression profiles and cluster according to the first two principal
796 components. (B) Volcano plot highlights most significantly (false discovery rate (FDR) <0.05)
797 regulated genes under $\Delta COLD_{diet}$ condition. (C) Heatmap of expression values shows that the
798 subgroups can be clearly separated by the top significant regulated genes. Abbreviations: HFD:
799 high fat diet; PC: principal component.

800 **Figure 3: Multi-layered insights into DMEGs under $COLD_{chow}$ condition.** (A) The scatter plot
801 displays the $\log_2$ fold changes (FC) in gene expression and DNA methylation signals for all
802 differentially methylated and expressed genes (DMEGs) in both gene body and promoter contexts
803 under the $COLD_{chow}$ condition. Colors indicate the direction of regulation. DMEGs with absolute
804 $\log_2$ FC >0.5 in expression and >1 in methylation signals are highlighted as significant, while
805 DMEGs in the 5% and 95% quantile of both differentially methylated position (DMP) and
806 differentially expressed gene (DEG) $\log_2$ FC signals are labeled. (B) The circos visualization
807 illustrates the DMEGs covering the top 100 significant differentially methylated regions (DMRs;
808 ranked by $\log_2$ FC). This plot integrates multiple layers of information from outer to inner ring: Dot
809 colors indicate the direction of regulation, while dot positions denote whether the DMR of the
810 DMEG is located in the gene body or promoter context (1); a stylized ideogram of chromosomes
811 provides a genomic reference frame; and a heatmap displays scaled log2 FC for both gene
812 expression and DNA methylation signals in gene body and promoter contexts for each DMEG (2).
813 (C) Overview of assigned cell types to the DMEGs, categorized as hypo up, hypo down, hyper up,
814 and hyper down. The color scale reflects the percentage of DMEGs, and the size of the dots reflects
815 the absolute number of DMEGs.

816 **Figure 4: Multi-layered insights into DMEGs under $COLD_{HFD}$ condition.** (A) The scatter plot
817 displays the $\log_2$ FC in gene expression and DNA methylation signals for all DMEGs in both gene
818 body and promoter contexts under the $COLD_{HFD}$ condition. Colors indicate the direction of

819 regulation. DMEGs with absolute $\log_2$ FC >0.5 in expression and >1 in methylation signal are
820 highlighted as significant, while DMEGs in the 5% and 95% quantile of both DMP and DEG $\log_2$
821 FC signals are labeled. (B) The circos visualization illustrates the DMEGs covering the top 100
822 most significant DMRs (ranked by $\log_2$ FC). This plot integrates multiple layers of information
823 from outer to inner ring: Dot colors indicate the direction of regulation, while dot positions denote
824 whether the DMR of the DMEG is located in the gene body or promoter context (1); a stylized
825 ideogram of chromosomes provides a genomic reference frame; and a heatmap displays scaled $\log_2$
826 FC for both gene expression and DNA methylation signals in gene body and promoter contexts for
827 each DMEG (2).

828 **Figure 5: Multi-layered insights into DMEGs under $\Delta COLD_{diet}$ condition.** (A) The scatter plot
829 displays the $\log_2$ FC in gene expression and DNA methylation signals for all DMEGs in both gene
830 body and promoter contexts under the $\Delta COLD_{diet}$ condition. Colors indicate the direction of
831 regulation. DMEGs with absolute $\log_2$ FC >0.5 in expression and >1 in methylation signals are
832 highlighted as significant, while DMEGs in the 5% and 95% quantile of both DMP and DEG $\log_2$
833 FC signals are labeled. (B) The circos visualization illustrates all detected DMEGs in their
834 respective DMRs. This plot integrates multiple layers of information from outer to inner ring: Dot
835 colors indicate the direction of regulation, while dot positions denote whether the DMR of the
836 DMEG is located in the gene body or promoter context (1); a stylized ideogram of chromosomes
837 provides a genomic reference frame; and a heatmap displays scaled $\log_2$ FC for both gene
838 expression and DNA methylation signals in gene body and promoter contexts for each DMEG (2).

839 **Figure 6: Pathway enrichment analysis of DMEGs for canonical pathways, diseases, and**
840 **biological functions.** Ingenuity Pathway Analysis (IPA) with enrichments of DMEGs were
841 categorized into four groups: those exhibiting similar regulation in both $COLD_{chow}$ and $COLD_{HFD}$
842 condition pairs, and those that are uniquely regulated in each individual condition ($\Delta COLD_{diet,}$
843 $COLD_{chow}$, and $COLD_{HFD}$). Top ten statistically significant enrichments are shown for canonical
844 pathways. More then ten enrichments are listed in case of p ties. Circle sizes reflect the number of
845 genes in each enrichment while the color highlights the activation z-score. Significance levels for
846 p after adjustment for multiple testing with Bonferroni-Holm are indicated as $p < 0.05$ (*), $p < 0.01$
847 (**).

848 **Figure 7: Overlap of methylation regulators in cold-induced BAT activation across dietary**
849 **conditions.** Upset plot displays the overlap of differentially expressed methylation regulators
850 detected for the $COLD_{chow}$, $COLD_{HFD}$, and $\Delta COLD_{diet}$ condition pairs. The scatterplot shows log2
851 FC values for each differentially expressed methylation regulator of the respective intersect in each
852 condition highlighted by coloring.

853

854 **Supplementary Figure legends**

855 **Suppl. Figure 1: Extended phenotyping of chow and HFD-fed mice housed at 30°C or 8°C.**
856 Overview thermal images from brown adipose tissue (BAT) (A), tail surface temperature (B) and
857 heat loss (Ttail – Trectal; (C) in chow and HFD-fed mice housed at thermoneutrality (30°C) or in
858 the cold (8°C) for 7 days. Average daily calory intake (D), final fasted blood glucose (E) and
859 absolute organ weights (F) of inguinal white adipose tissue (iWAT), epididymal white adipose
860 tissue (eWAT), BAT and liver of chow and HFD-fed mice housed at thermoneutrality (30°C) or in
861 the cold (8°C) for 7 days. N = 7-8 per condition. Statistical significance was evaluated one-way
862 ANOVA with Tukey's post-hoc test (B-D) or uncorrected Fischer's LDS (E) or two-way ANOVA
863 with uncorrected Fischer's LDS (F). $p < 0.05$ (*), $p < 0.01$ (**), $p < 0.001$ (***).

864 **Suppl. Figure 2: Differential gene expression in response to cold exposure in chow diet and**
865 **HFD-fed mice.** Summary of differential gene expression signals for cold-induced BAT activation
866 in (A, B) normal-weight control mice ($COLD_{chow}$) and (C, D) high fat diet (HFD)-induced obese
867 mice ($COLD_{HFD}$). Volcano plots (A, C) and heatmaps (B, D) display differentially expressed genes
868 (DGEs) based on $\log_2$ fold change (FC) and false discovery rate (FDR) signals and show clustering
869 of the top 25 DGEs, respectively.

870 **Suppl. Figure 3: Overlap of DEGs in the $COLD_{chow}$ condition with published data.** Upset plots
871 show the intersection of DEGs from the $COLD_{chow}$ condition and DEGs reported by Tayler et al.
872 (2024) [60] for chow-fed male mice (8°C vs 28°C), categorized by positive (up) and negative
873 (down) regulation. DEGs with adj. $P > 0.05$ were compared. Set size indicates the total number of
874 DEGs.

875 **Suppl. Figure 4: Overlap of DEGs and DMEGs between the $COLD_{chow}$ and**
876 **$COLD_{HFD}$ conditions.** Upset plots display the overlap of (A) DEGs and (B) differentially
877 methylated and expressed genes (DMEGs) for the $COLD_{chow}$ and $COLD_{HFD}$ condition pairs,
878 categorized by positive (up) and negative (down) regulation. Significant DEGs or DMEGs that
879 show the same and contrary regulatory direction in both conditions are highlighted in red and black
880 respectively. Those significant only in the $COLD_{chow}$ condition are shown in blue, while those
881 significant only in the $COLD_{HFD}$ condition are marked in yellow. Genes are counted uniquely, even
882 though multiple DMEGs may be associated with the same gene. Set size indicates the total number
883 of DEGs or DMEGs.

884 **Suppl. Figure 5: In vitro validation of DNA methylation affecting expression of candidate**
885 **genes. (**A) Inhibition of DNA methylation using indicated concentrations of Aza in mouse
886 immortalized (imBA, left) and primary brown adipocytes (right). Gene expression was analyzed
887 by qPCR, N = 6-10 per condition. (B) Induction of DNA hypermethylation using indicated
888 concentrations of SAM in mouse imBA. Gene expression was analyzed by qPCR, n = 3-5 per
889 condition. Statistical significance was evaluated by two-way ANOVA with uncorrected Fischer's
890 LSD. $p < 0.05$ (*), $p < 0.01$ (**), $p < 0.001$ (***).

891 **Suppl. Figure 6: Overlapping DMEGs between *$COLD_{chow}$* and *$COLD_{HFD}$*.** The scatter plot
892 displays the $\log_2$ FC in gene expression and DNA methylation signals for all DMEGs which
893 overlap in both *$COLD_{chow}$* and *$COLD_{HFD}$* condition. Colors correspond to highlights in Suppl.
894 Figure 3. DMEGs with absolute $\log_2$ FC >0.5 in expression and >1 in methylation signals are
895 shown, while DMEGs in the 5% and 95% quantile of both DMP and DEG $\log_2$ FC signals are
896 labeled.

897 **Suppl. Figure 7: DMEGs that are specifically regulated within each condition.** The scatter plot
898 displays the $\log_2$ FC in gene expression and DNA methylation signals for all DMEGs which are
899 specifically regulated in both *$COLD_{chow}$* and *$COLD_{HFD}$* conditions. Colors correspond to highlights
900 in Suppl. Figure 3. DMEGs with absolute $\log_2$ FC >0.5 in expression and >1 in methylation signals
901 are shown, while DMEGs in the 5% and 95% quantile of both DMP and DEG $\log_2$ FC signals are
902 labeled.

903 **Supplementary Table legends**

904 **Suppl. Table 1:** Overview of primers used for PCR.

905 **Suppl. Table 2:** Overview of significant (FDR <0.05) DEGs for the *$COLD_{chow}$* contrast. DEGs that
906 overlap with Tayler et al. (2024) [60] (chow-fed mice, 8°C vs 28°C) are listed.

907 **Suppl. Table 3:** Overview of significant (FDR <0.05) DEGs for the *$COLD_{HFD}$* contrast.

908 **Suppl. Table 4:** Overview of significant (FDR <0.05) DEGs for the *$\Delta COLD_{diet}$* condition.

909 **Suppl. Table 5:** Overview of DMEGs in the *$COLD_{chow}$* contrast with absolute expression $\log_2$ FC
910 >0.5 and absolute methylation $\log_2$ FC >1, including the cell type assignment derived from single-
911 cell RNAseq data obtained from [38].

912 **Suppl. Table 6:** Overview of DMEGs in the *$COLD_{HFD}$* contrast with absolute expression $\log_2$ FC
913 >0.5 and absolute methylation $\log_2$ FC >1.

914 **Suppl. Table 7:** Overview of DMEGs in the *$\Delta COLD_{diet}$* contrast with absolute expression $\log_2$ FC
915 >0.5 and absolute methylation $\log_2$ FC >1.

916 **Suppl. Table 8:** Significant IPA enrichment (before p adjustment) for canonical pathways
917 categorized by four groups: those exhibiting similar regulation in both *$COLD_{HFD}$* and *$COLD_{chow}$*
918 condition pairs, and those that are uniquely regulated in each individual condition (*$\Delta COLD_{diet}$*,
919 *$COLD_{chow}$*, and *$COLD_{HFD}$*.)

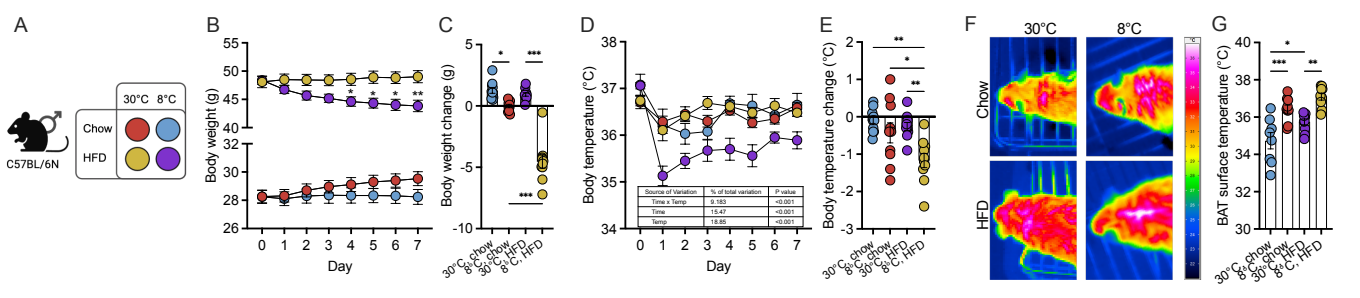
A
30°C
8°C
Chow
HFD
C57BL/6N
B
Body weight (g)
Day
C
Body weight change (g)
30°C, chow
8°C, chow
30°C, HFD
8°C, HFD
D
Body temperature (°C)
Day
Source of Variation | % of total variation | P value
Time x Temp | 9.183 | <0.001
Time | 15.47 | <0.001
Temp | 18.55 | <0.001
E
Body temperature change (°C)
F
30°C
8°C
Chow
HFD
°C
G
BAT surface temperature (°C)

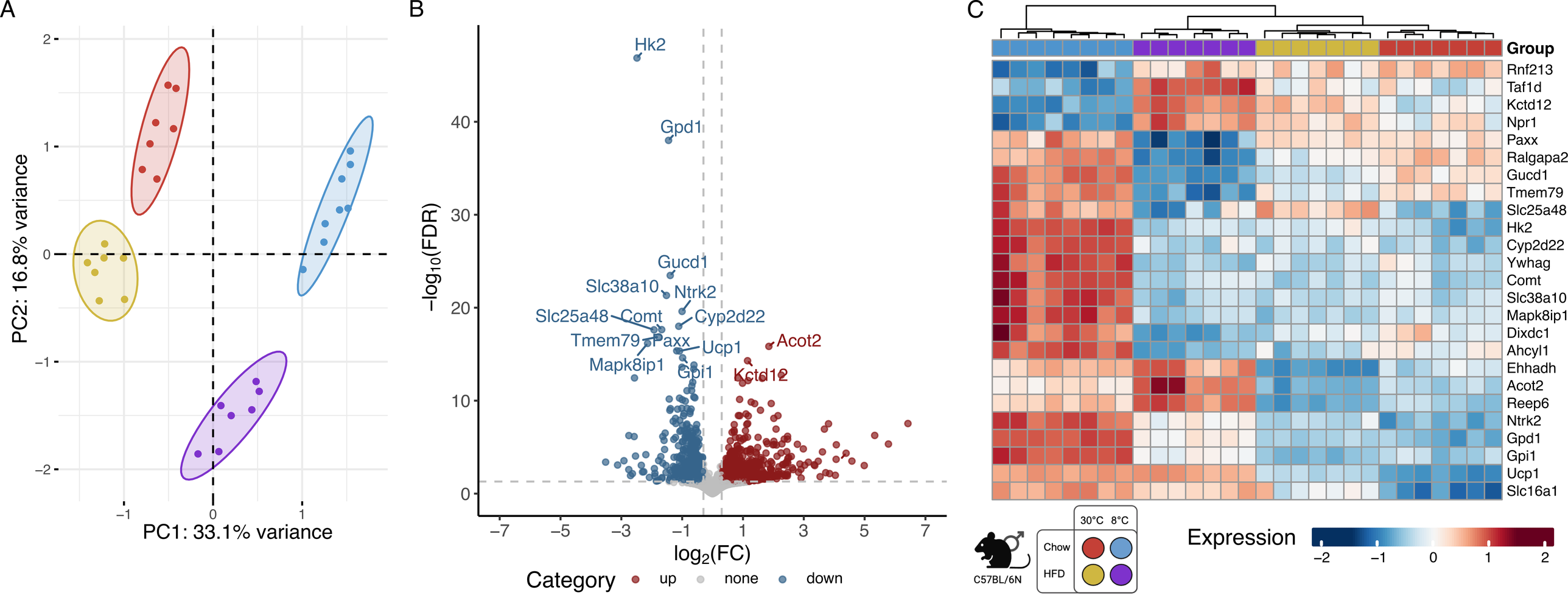
A
PC2: 16.8% variance
PC1: 33.1% variance
B
Hk2
Gpd1
Gucd1
Slc38a10
Ntrk2
Slc25a48
Comt
Cyp2d22
Tmem79
Paxx
Ucp1
Acot2
Mapk8ip1
Gpi1
Kctd12
−log10(FDR)
log2(FC)
Category
up
none
down
C
Group
Rnf213
Taf1d
Kctd12
Npr1
Paxx
Ralgapa2
Gucd1
Tmem79
Slc25a48
Hk2
Cyp2d22
Ywhag
Comt
Slc38a10
Mapk8ip1
Dixdc1
Ahcyl1
Ehhadh
Acot2
Reep6
Ntrk2
Gpd1
Gpi1
Ucp1
Slc16a1
C57BL/6N
30°C
8°C
Chow
HFD
Expression

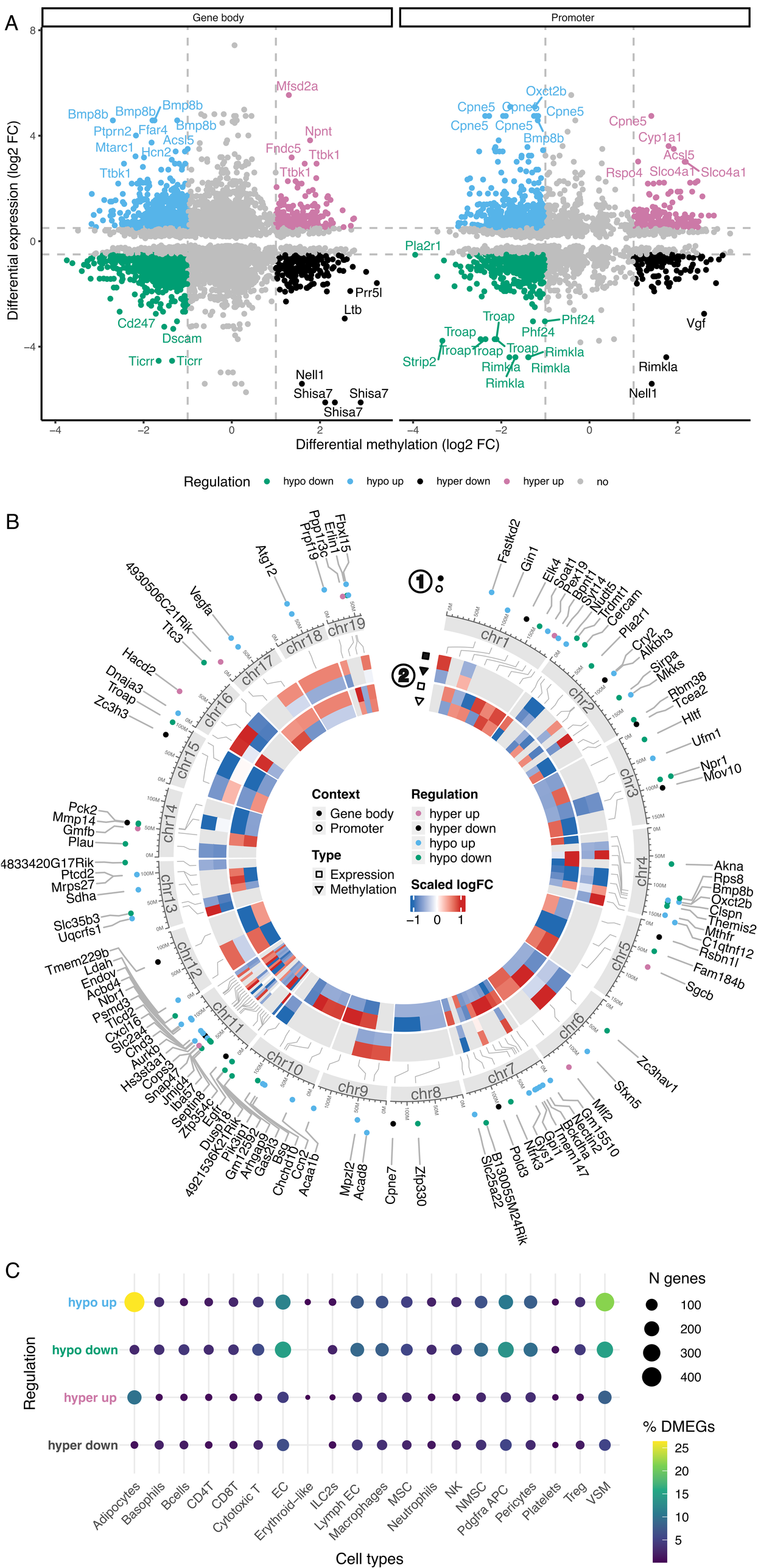
A
Gene body
Promoter
Differential expression (log2 FC)
Differential methylation (log2 FC)
Mfsd2a
Bmp8b
Ptprn2
Ffar4
Acsl5
Mtarc1
Hcn2
Ttbk1
Npnt
Fndc5
Cd247
Dscam
Ticrr
Prr5l
Ltb
Nell1
Shisa7
Oxct2b
Cpne5
Cyp1a1
Rspo4
Slco4a1
Pla2r1
Troap
Phf24
Strip2
Rimkla
Vgf
Regulation
hypo down
hypo up
hyper down
hyper up
no
B
Context
Gene body
Promoter
Type
Expression
Methylation
Regulation
hyper up
hyper down
hypo up
hypo down
Scaled logFC
−1 0 1
chr1
chr2
chr3
chr4
chr5
chr6
chr7
chr8
chr9
chr10
chr11
chr12
chr13
chr14
chr15
chr16
chr17
chr18
chr19
Fastkd2
Gin1
Elk4
Soat1
Pex19
Bpnt1
Syt14
Nudt5
Trdmt1
Cercam
Pla2r1
Cry2
Alkbh3
Sirpa
Mkks
Rbm38
Tcea2
Hltf
Ufm1
Npr1
Mov10
Akna
Rps8
Bmp8b
Oxct2b
Clspn
Themis2
Mthfr
C1qtnf12
Rsbn1l
Fam184b
Sgcb
Zc3hav1
Sfxn5
Mlf2
Gm15510
Nectin2
Bckdha
Tmem147
Gpi1
Gys1
Nfrk3
Pold3
B130055M24Rik
Slc25a22
Zfp330
Cpne7
Mpzl2
Acad8
Acaa1b
Ccn2
Chchd10
Bsg
Gas2l3
Arhgap9
Gm12592
Pik3ip1
4921536K21Rik
Dusp18
Egfr
Zfp354c
Septin8
Iba57
Jmjd4
Snap47
Cops3
Hs3st3a1
Aurkb
Chd3
Slc2a4
Cxcl16
Tlcd2
Psmd3
Nbr1
Acbd4
Endov
Ldah
Tmem229b
Slc35b3
Uqcrfs1
Sdha
Mrps27
Ptcd2
4833420G17Rik
Plau
Gmfb
Mmp14
Pck2
Zc3h3
Troap
Dnaja3
Hacd2
Ttc3
Vegfa
4930506C21Rik
Atg12
Prpf19
Ppp1r3c
Erlin1
Fbxl15
①
②
C
Regulation
hypo up
hypo down
hyper up
hyper down
Adipocytes
Basophils
Bcells
CD4T
CD8T
Cytotoxic T
EC
Erythroid-like
ILC2s
Lymph EC
Macrophages
MSC
Neutrophils
NK
NMSC
Pdgfra APC
Pericytes
Platelets
Treg
VSM
Cell types
N genes
100
200
300
400
% DMEGs
25
20
15
10
5

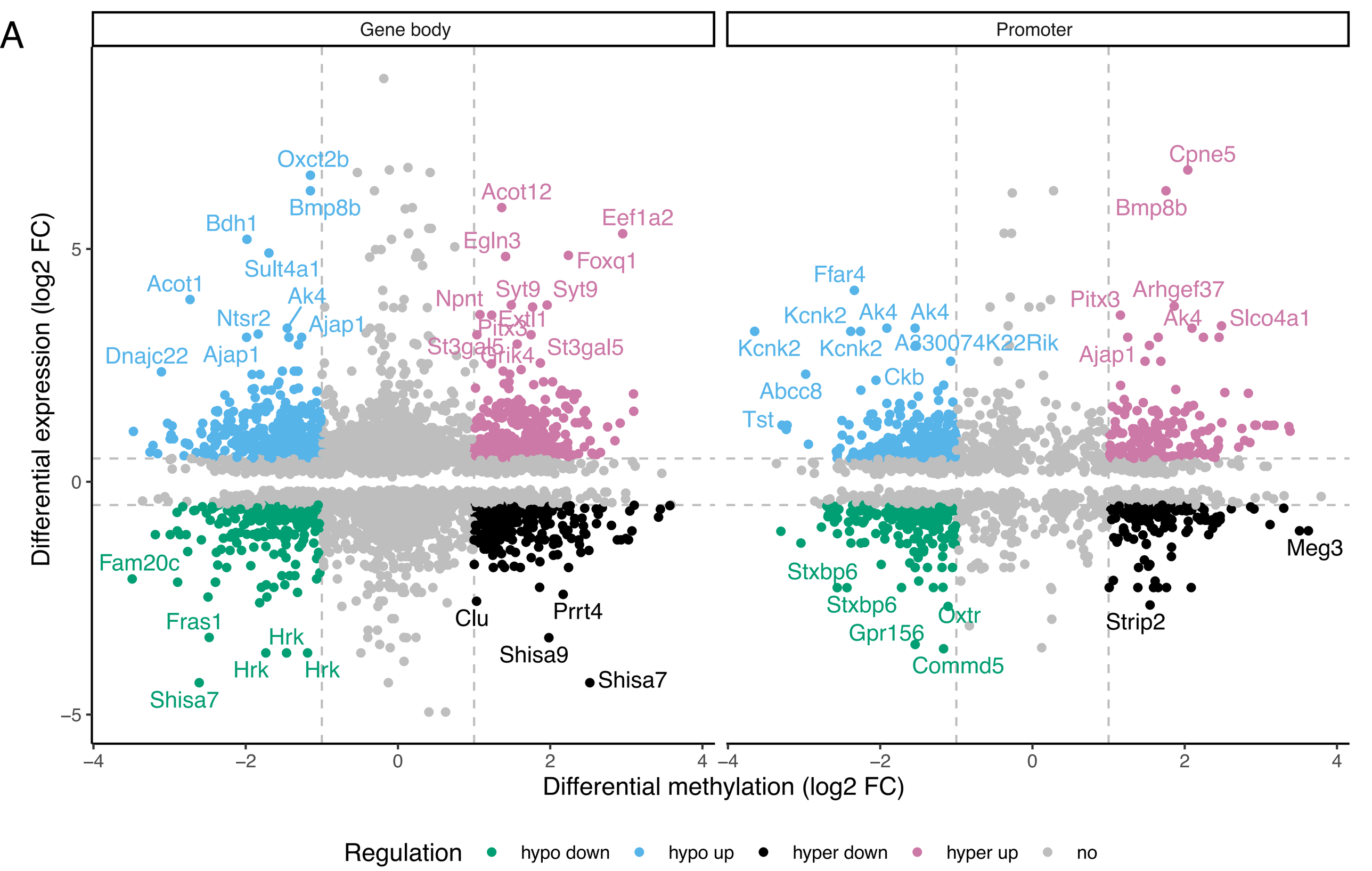
A
Gene body
Promoter
Differential expression (log2 FC)
Differential methylation (log2 FC)
Oxct2b
Bmp8b
Bdh1
Sult4a1
Acot1
Ak4
Ntsr2
Ajap1
Dnajc22
Ajap1
Acot12
Egln3
Eef1a2
Foxq1
Npnt
Syt9
Syt9
Extl1
Pitx3
St3gal5
Grik4
St3gal5
Fam20c
Fras1
Hrk
Hrk
Hrk
Shisa7
Clu
Prrt4
Shisa9
Shisa7
Cpne5
Bmp8b
Ffar4
Kcnk2
Ak4
Ak4
Kcnk2
Kcnk2
A330074K22Rik
Ckb
Abcc8
Tst
Pitx3
Arhgef37
Ak4
Slco4a1
Ajap1
Meg3
Stxbp6
Stxbp6
Oxtr
Gpr156
Commd5
Strip2
Regulation
hypo down
hypo up
hyper down
hyper up
no

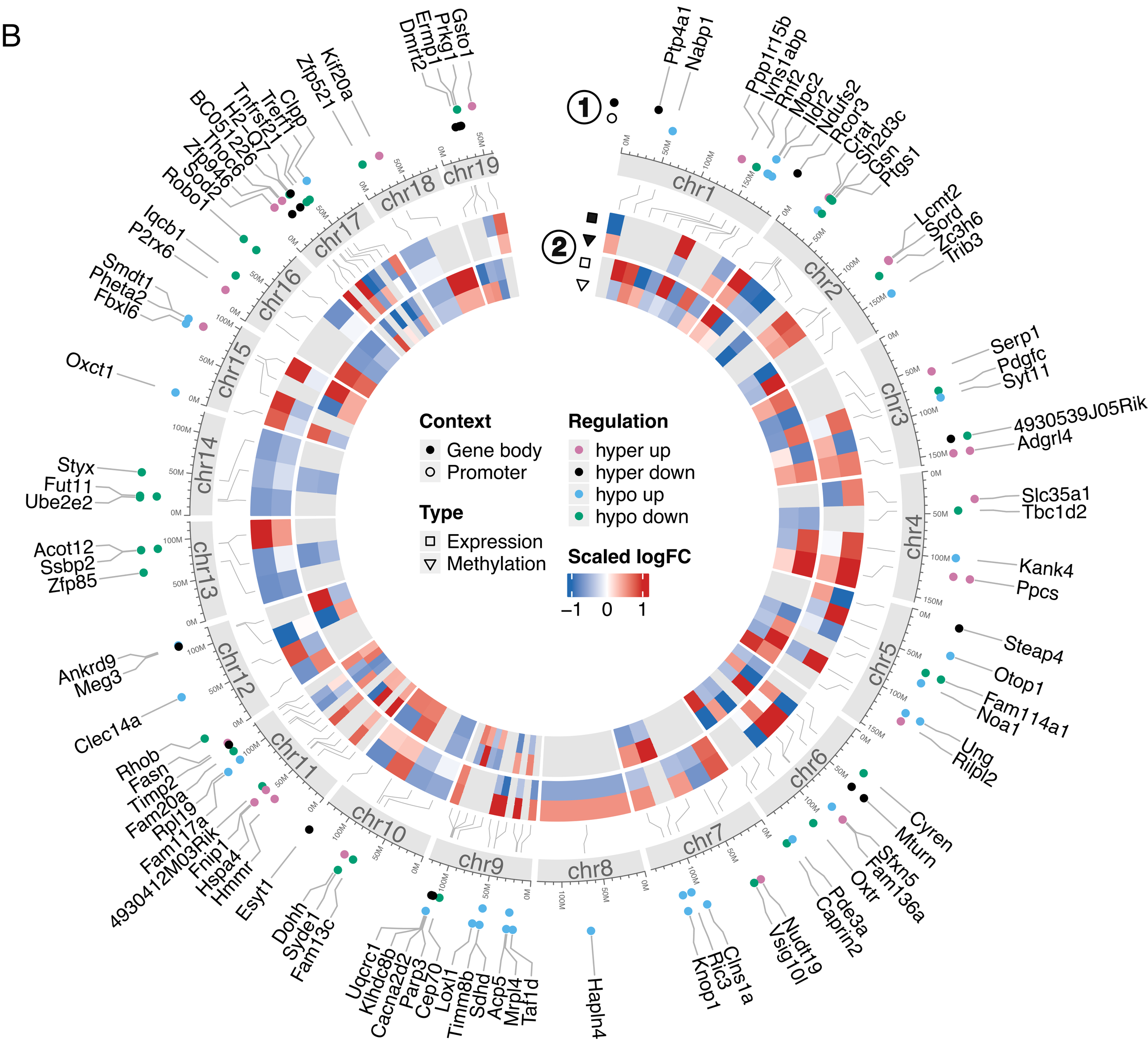
B
Context
Gene body
Promoter
Type
Expression
Methylation
Regulation
hyper up
hyper down
hypo up
hypo down
Scaled logFC
–1
0
1
chr1
chr2
chr3
chr4
chr5
chr6
chr7
chr8
chr9
chr10
chr11
chr12
chr13
chr14
chr15
chr16
chr17
chr18
chr19
Gsto1
Prkg1
Ermp1
Dmrt2
Kif20a
Zfp521
Clpp
Trerf1
Tnfrsf21
H2-Q7
BC051226
Thoc6
Zfp946
Sod2
Robo1
Iqcb1
P2rx6
Smdt1
Pheta2
Fbxl6
Oxct1
Styx
Fut11
Ube2e2
Acot12
Ssbp2
Zfp85
Ankrd9
Meg3
Clec14a
Rhob
Fasn
Timp2
Fam20a
Rpl19
Fam117a
4930412M03Rik
Fnip1
Hspa4
Hmmr
Esyt1
Dohh
Syde1
Fam13c
Uqcrc1
Klhdc8b
Cacna2d2
Parp3
Cep70
Loxl1
Timm8b
Sdhd
Acp5
Mrpl4
Taf1d
Hapln4
Clns1a
Ric3
Knop1
Nudt19
Vsig10l
Pde3a
Caprin2
Oxtr
Sfxn5
Fam136a
Cyren
Mturn
Ung
Rilpl2
Fam114a1
Noa1
Otop1
Steap4
Kank4
Ppcs
Slc35a1
Tbc1d2
4930539J05Rik
Adgrl4
Serp1
Pdgfc
Syt11
Lcmt2
Sord
Zc3h6
Trib3
Ptp4a1
Nabp1
Ppp1r15b
Ivns1abp
Rnf2
Mpc2
Ildr2
Ndufs2
Rcor3
Crat
Sh2d3c
Gsn
Ptgs1

A

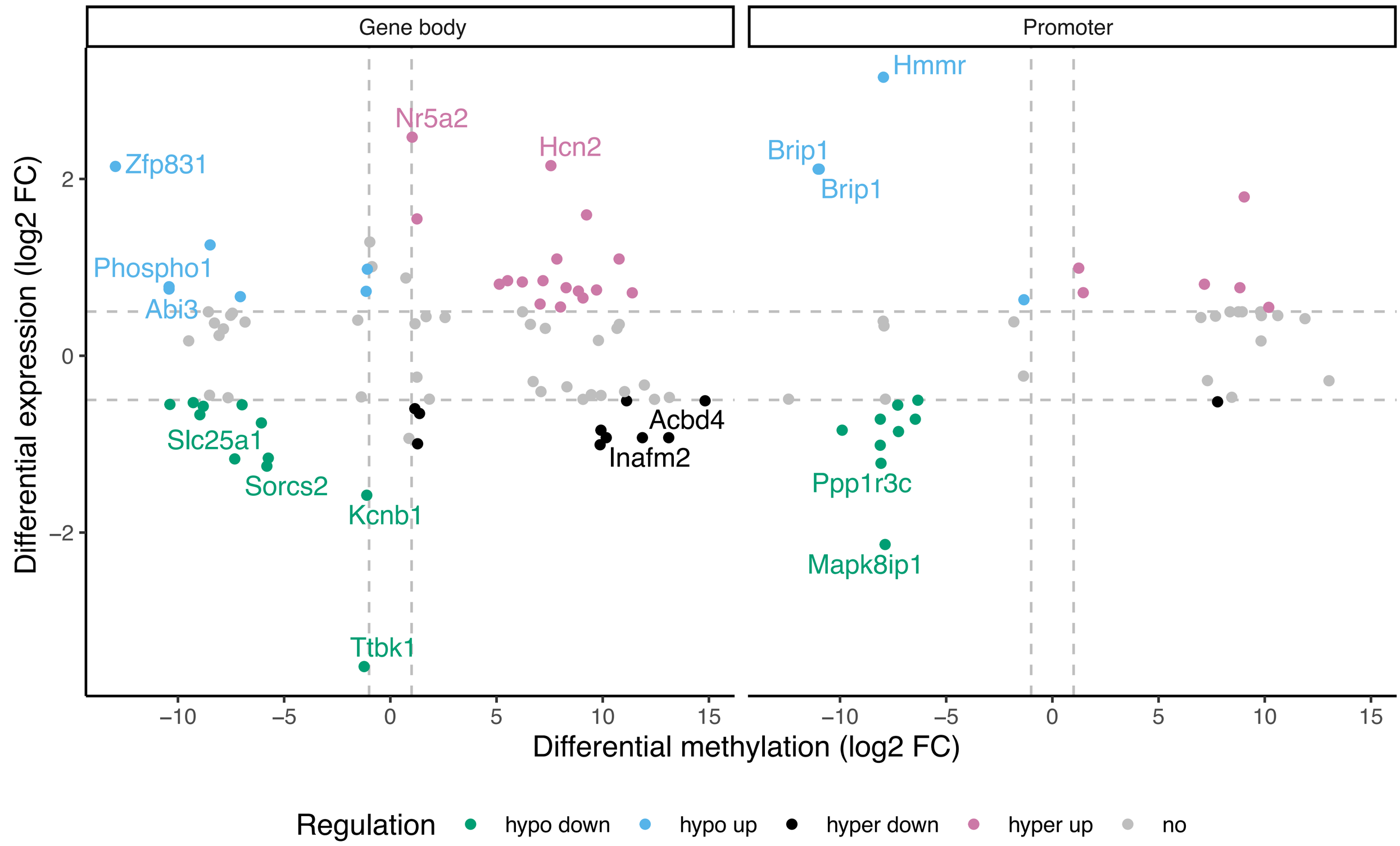
Gene body
Promoter
Differential expression (log2 FC)
Differential methylation (log2 FC)
Zfp831
Phospho1
Abi3
Nr5a2
Hcn2
Hmmr
Brip1
Brip1
Slc25a1
Sorcs2
Kcnb1
Acbd4
Inafm2
Ppp1r3c
Mapk8ip1
Ttbk1
Regulation
hypo down
hypo up
hyper down
hyper up
no

B

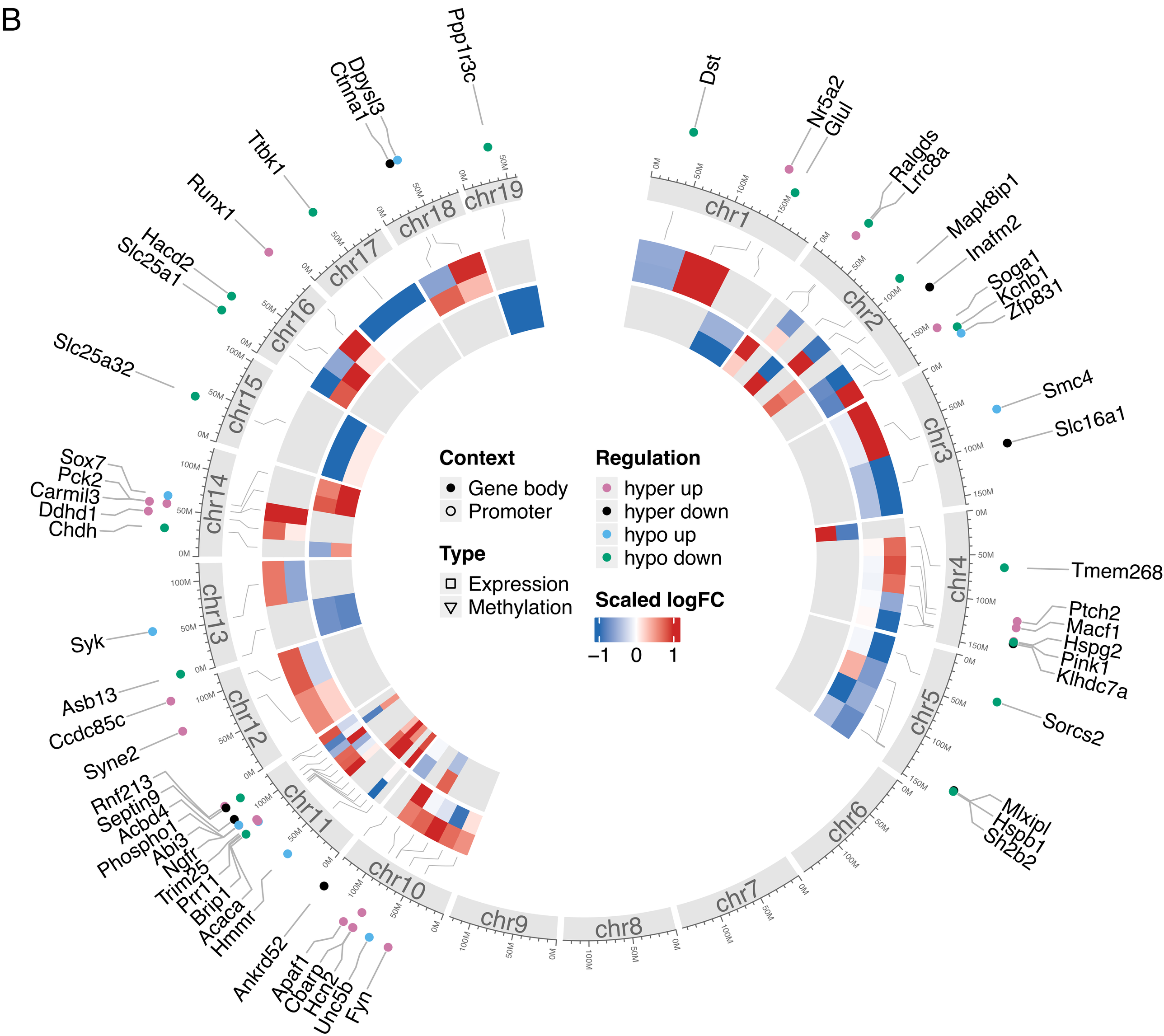
Ppp1r3c
Dpysl3
Ctnna1
Ttbk1
Runx1
Hacd2
Slc25a1
Slc25a32
Sox7
Pck2
Carmil3
Ddhd1
Chdh
Syk
Asb13
Ccdc85c
Syne2
Rnf213
Septin9
Acbd4
Phospho1
Abi3
Ngfr
Trim25
Prr11
Brip1
Acaca
Hmmr
Ankrd52
Apaf1
Cbarp
Hcn2
Unc5b
Fyn
Dst
Nr5a2
Glul
Ralgds
Lrrc8a
Mapk8ip1
Inafm2
Soga1
Kcnb1
Zfp831
Smc4
Slc16a1
Tmem268
Ptch2
Macf1
Hspg2
Pink1
Klhdc7a
Sorcs2
Mlxipl
Hspb1
Sh2b2
chr1
chr2
chr3
chr4
chr5
chr6
chr7
chr8
chr9
chr10
chr11
chr12
chr13
chr14
chr15
chr16
chr17
chr18
chr19
Context
Gene body
Promoter
Type
Expression
Methylation
Regulation
hyper up
hyper down
hypo up
hypo down
Scaled logFC
−1
0
1

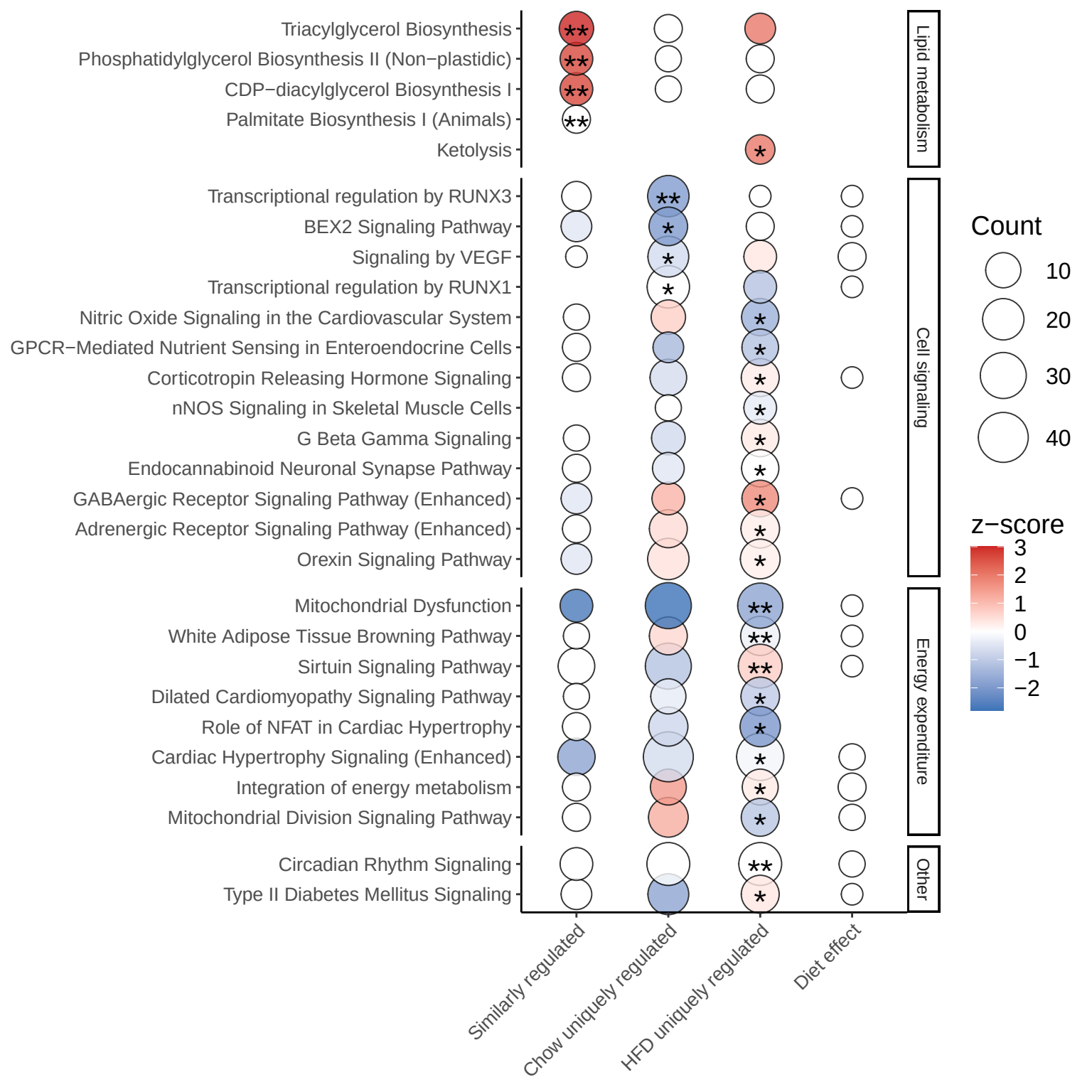
Triacylglycerol Biosynthesis
Phosphatidylglycerol Biosynthesis II (Non−plastidic)
CDP−diacylglycerol Biosynthesis I
Palmitate Biosynthesis I (Animals)
Ketolysis
Transcriptional regulation by RUNX3
BEX2 Signaling Pathway
Signaling by VEGF
Transcriptional regulation by RUNX1
Nitric Oxide Signaling in the Cardiovascular System
GPCR−Mediated Nutrient Sensing in Enteroendocrine Cells
Corticotropin Releasing Hormone Signaling
nNOS Signaling in Skeletal Muscle Cells
G Beta Gamma Signaling
Endocannabinoid Neuronal Synapse Pathway
GABAergic Receptor Signaling Pathway (Enhanced)
Adrenergic Receptor Signaling Pathway (Enhanced)
Orexin Signaling Pathway
Mitochondrial Dysfunction
White Adipose Tissue Browning Pathway
Sirtuin Signaling Pathway
Dilated Cardiomyopathy Signaling Pathway
Role of NFAT in Cardiac Hypertrophy
Cardiac Hypertrophy Signaling (Enhanced)
Integration of energy metabolism
Mitochondrial Division Signaling Pathway
Circadian Rhythm Signaling
Type II Diabetes Mellitus Signaling
Lipid metabolism
Cell signaling
Energy expenditure
Other
Similarly regulated
Chow uniquely regulated
HFD uniquely regulated
Diet effect
Count
10
20
30
40
z−score
3
2
1
0
−1
−2

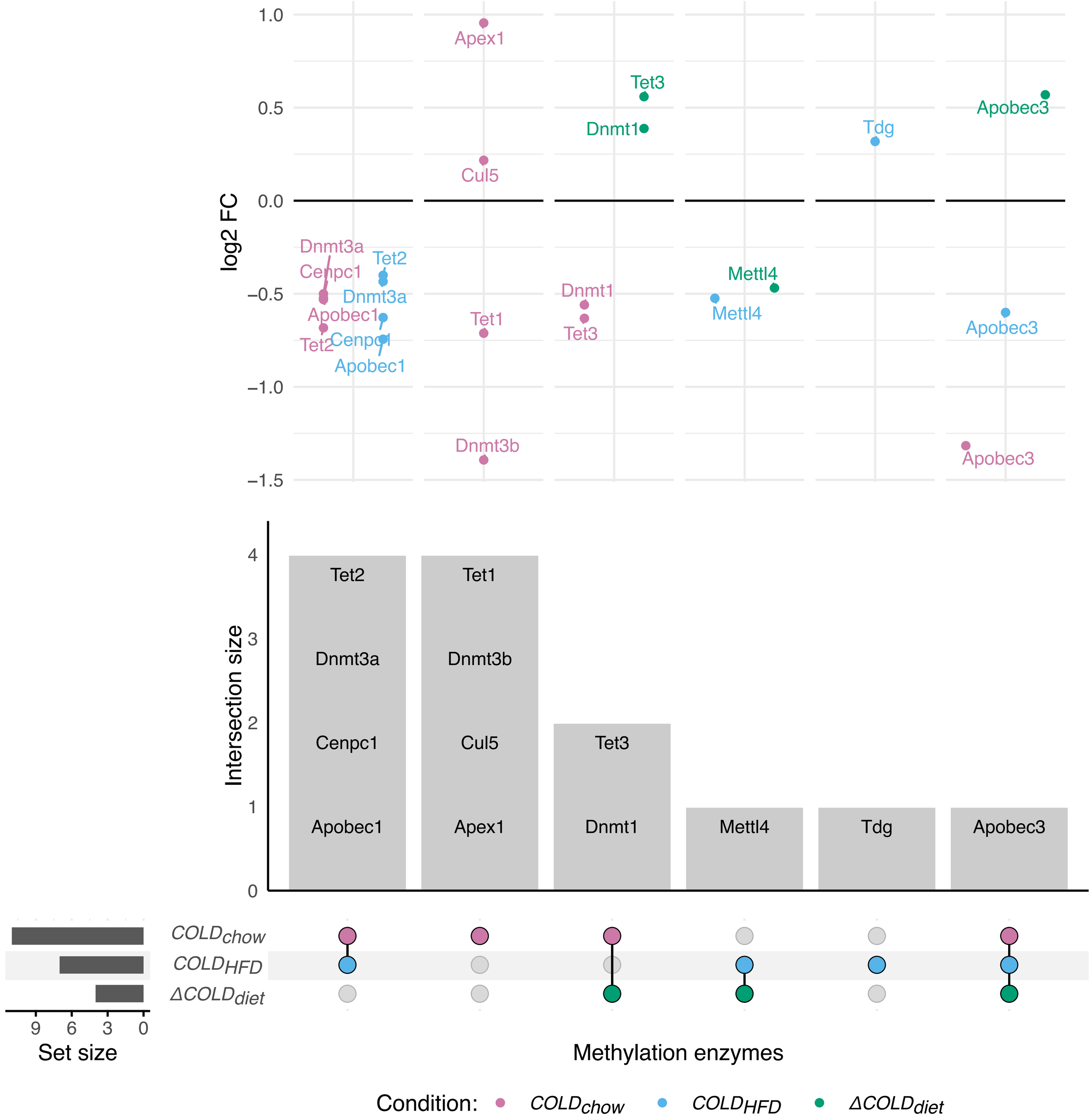
log2 FC
1.0
0.5
0.0
−0.5
−1.0
−1.5
Apex1
Cul5
Dnmt3b
Dnmt3a
Cenpc1
Apobec1
Tet2
Cenpc1
Dnmt3a
Apobec1
Tet2
Tet1
Tet3
Dnmt1
Dnmt1
Tet3
Mettl4
Mettl4
Tdg
Apobec3
Apobec3
Apobec3
Intersection size
4
3
2
1
0
Tet2
Dnmt3a
Cenpc1
Apobec1
Tet1
Dnmt3b
Cul5
Apex1
Tet3
Dnmt1
Mettl4
Tdg
Apobec3
COLDchow
COLDHFD
ΔCOLDdiet
9
6
3
0
Set size
Methylation enzymes
Condition:
COLDchow
COLDHFD
ΔCOLDdiet